Astronomy & Astrophysics manuscript no. o3imbh
August 27, 2021

Search for intermediate mass black hole binaries in the third observing run of Advanced LIGO and Advanced Virgo

The LIGO Scientific Collaboration, the Virgo Collaboration, and the KAGRA Collaboration (full author list in Appendix C)

1

August 27, 2021

ABSTRACT

Intermediate-mass black holes (IMBHs) span the approximate mass range 100–10^5 $M_\odot$, between black holes (BHs) formed by stellar collapse and the supermassive BHs at the centers of galaxies. Mergers of IMBH binaries are the most energetic gravitational-wave sources accessible by the terrestrial detector network. Searches of the first two observing runs of Advanced LIGO and Advanced Virgo did not yield any significant IMBH binary signals. In the third observing run (O3), the increased network sensitivity enabled the detection of GW190521, a signal consistent with a binary merger of mass $\sim 150\,M_\odot$ providing direct evidence of IMBH formation. Here we report on a dedicated search of O3 data for further IMBH binary mergers, combining both modelled (matched filter) and model independent search methods. We find some marginal candidates, but none are sufficiently significant to indicate detection of further IMBH mergers. We quantify the sensitivity of the individual search methods and of the combined search using a suite of IMBH binary signals obtained via numerical relativity, including the effects of spins misaligned with the binary orbital axis, and present the resulting upper limits on astrophysical merger rates. Our most stringent limit is for equal mass and aligned spin BH binary of total mass $200 M_\odot$ and effective aligned spin 0.8 at $0.056\,\mathrm{Gpc^{-3}yr^{-1}}$ (90% confidence), a factor of 3.5 more constraining than previous LIGO-Virgo limits. We also update the estimated rate of mergers similar to GW190521 to $0.08\,\mathrm{Gpc^{-3}yr^{-1}}$.

Key words. Gravitational waves, black holes, black hole physics

1. Introduction

Black holes are classified according to their masses: stellar-mass black holes (BHs) are those with mass below $\sim 100\,M_\odot$, formed by stellar collapse, while supermassive BHs (Ferrarese & Ford 2005) at the centers of galaxies have masses above $10^5\,M_\odot$. Between stellar-mass and supermassive BHs is the realm of intermediate mass black holes (IMBHs) – BHs with masses in the range $100-10^5\,M_\odot$ (van der Marel 2004; Miller & Colbert 2004; Ebisuzaki et al. 2001; Koliopanos 2017; Inayoshi et al. 2020).

Stellar evolution models suggest that BHs with mass up to $\sim 65\,M_\odot$ are the result of core-collapse of massive stars (Woosley 2017; Giacobbo et al. 2018; Woosley 2019; Farmer et al. 2019; Mapelli et al. 2020; Farmer et al. 2020). The final fate of the star is determined by the mass of the helium core alone. Stars with helium core mass in the range $\sim 32-64\,M_\odot$ undergo pulsational pair-instability leaving behind remnant BHs of mass below $\sim 65\,M_\odot$ (Fowler & Hoyle 1964; Barkat et al. 1967). When the helium core mass is in the range $\sim 64-135\,M_\odot$, pair-instability drives the supernova explosion and leaves no remnant; while stars with helium core mass greater than $\sim 135\,M_\odot$ are expected to directly collapse to intermediate-mass BHs. Thus, pair-instability (PI) prevents the formation of heavier BHs from core-collapse, and suggests a mass gap between $\sim 65-120\,M_\odot$ in the BH population known as PI supernova (PISN) mass gap (Bond et al. 1984; Woosley et al. 2007; Woosley & Heger 2021). Possible IMBH formation channels also include the direct collapse of massive first-generation, low-metallicity Population III stars (Fryer et al. 2001; Heger et al. 2003; Spera & Mapelli 2017; Madau & Rees 2001; Heger & Woosley 2002), and multiple, hierarchical collisions of stars in dense young star clusters (Miller & Hamilton 2002; O'Leary et al. 2006; Giersz et al. 2015; Mapelli 2016), among others. It is not currently known how supermassive black holes form. Hierarchical merger of IMBH systems in a dense environment is among the putative formation channels for supermassive BHs (King & Dehnen 2005; Volonteri 2010; Mezcua 2017; Koliopanos 2017).

Several IMBH candidates are suggested by electromagnetic observations, but lack conclusive confirmation (Greene et al. 2020). Observations include direct kinematical measurement of the mass of the central BH in massive star clusters and galaxies (Mezcua 2017; Miller & Hamilton 2002; Atakan Gurkan et al. 2004; Anderson & van der Marel 2010; Baumgardt et al. 2003; Pasham et al. 2015; Vitral & Mamon 2021). Other possible evidence for IMBH includes extrapolation of scaling relations between the masses of host galaxies and their central supermassive BH to the mass range of globular clusters (Graham 2012; Graham & Scott 2013; Kormendy & Ho 2013). In addition, observations of characteristic imprints on the surface brightness, mass-to-light ratio and/or line-of-sight velocities also suggest that dense globular clusters harbour IMBHs (van den Bosch et al. 2006; Gebhardt et al. 2005; Noyola et al. 2008; Lützgendorf et al. 2011; Kızıltan et al. 2017). Controversy exists regarding the interpretation of these observations, as some of them can also be explained by a high concentration of stellar-mass BHs or the presence of binaries (Baumgardt et al. 2003; Anderson & van der Marel 2010; Lanzoni et al. 2013). Empirical mass scaling relations of quasi-periodic oscillations in luminous X-ray sources have also provided evidence for IMBHs (Remillard & McClintock 2006). Ultraluminous X-ray sources exceed the Eddington luminosity of an accreting stellar-mass BH (Kaaret et al. 2017; Farrell et al. 2009). An accreting IMBH is a favored explanation in several cases (Kaaret et al. 2001; Miller & Colbert 2004). However, neutron stars or stellar-mass black holes emitting above their Eddington luminosity could also account for such observations (Bachetti et al. 2014; Israel et al. 2017). The strongest IMBH candidate amongst them is HLX-1, an hyper-luminous X-ray source indicating an IMBH mass of $\sim 0.3 - 30 \times 10^4\, M_\odot$ (Farrell et al. 2009; Godet et al. 2009; Servillat et al. 2011; Webb et al. 2012; Cseh et al. 2015; Soria et al. 2012). In Lin et al. (2018), an intermediate-mass black hole candidate was found in a tidal disruption event in a massive star cluster. More recently, in Paynter et al. (2021), there was a claim of an IMBH detection through a gravitationally lensed gamma ray burst.

The Advanced LIGO (Aasi et al. 2015) and Advanced Virgo (Acernese et al. 2015) interferometric gravitational wave (GW) detectors have completed three observing runs between September 2015 and March 2020. The third observing run of Advanced LIGO and Advanced Virgo, O3, extended from April 1st, 2019, 15:00 UTC to March 27th, 2020 17:00 UTC. The recently released second gravitational-wave transient catalog provided a comprehensive summary of significant compact binary coalescence events observed up to October 1st, 2019 (Abbott et al. 2021a), reporting a total of 50 events. The corresponding binary black hole (BBH) population analysis of Abbott et al. (2021c) indicates that 99% of primary BH masses lie below $m_{99\%} \sim 60\,\mathrm{M}_\odot$: thus, the large majority of merging BH have masses below a limit of $\sim 65\,\mathrm{M}_\odot$ consistent with expectations from PI.

Near the beginning of O3, an unusually high mass black hole coalescence, GW190521 (Abbott et al. 2020b), was detected. This GW signal was consistent with a coalescence of black holes of $85^{+21}_{-14}\mathrm{M}_\odot$, and $66^{+17}_{-18}\mathrm{M}_\odot$ which resulted in a remnant black hole of $142^{+28}_{-16}\mathrm{M}_\odot$ falling in the mass range of intermediate-mass black holes[1] GW190521 provided the first conclusive evidence for the formation of an IMBH below $10^3\,\mathrm{M}_\odot$. It is a massive binary black hole system with an IMBH remnant and a primary BH in the PISN mass gap with high confidence (Abbott et al. 2020c, although see Fishbach & Holz 2020 and Nitz & Capano 2021 for an alternative interpretation). The discovery triggered a variety of investigations regarding the evolution models and the subsequent mass gap in the BH population. It also suggested a possibility of the formation of massive BHs ($>100\,\mathrm{M}_\odot$) via hierarchical merger scenario in a dense environment (Abbott et al. 2020c; Kimball et al. 2021).

The Advanced LIGO - Advanced Virgo detectors are sensitive to the lower end of the IMBH binary mass range, potentially making IMBHs detectable out to cosmological distances, as is evident from GW190521. Observation of IMBH binary systems are not only interesting for massive BH formation channels, but they act as a perfect laboratory to test general relativity (Abbott et al. 2016b; Yunes et al. 2016; Yunes & Siemens 2013; Gair et al. 2013). Massive BH coalescences produce louder mergers and ringdown signals in the sensitive band of the advanced GW detectors. Furthermore, these can display prominent higher-order modes that confer GWs a more complex morphology that can significantly deviate from a canonical chirp (Calderon Bustillo et al. 2020). Observations of higher-order modes help to test general relativity and fundamental properties of BHs such as the no-hair theorem (Kamaretsos et al. 2012; Meidam et al. 2014; Thrane et al. 2017; Carullo et al. 2018) and BH kick measurements (Gonzalez et al. 2007; Campanelli et al. 2007; Calderón Bustillo et al. 2018). These IMBHs might be multi-band events observable by both LIGO/Virgo and *LISA* (Amaro-Seoane et al. 2017), and could provide novel probes of cosmology and contribute to the stochastic background (Fregeau et al. 2006; Miller 2009; Jani et al. 2020; Ezquiaga & Holz 2021).

The GW signal from a massive BBH coalescence is evident as a short-duration waveform with little inspiral and mostly merger-ringdown signal, falling in the low-frequency region of the advanced detectors. With initial GW detectors (Abadie et al. 2012b; Aasi et al. 2014), the IMBH binary searches were restricted to probe the merger-ringdown phase of the coalescing BBH system, using the model waveform independent coherent WaveBurst (cWB) (Klimenko & Mitselmakher 2004; Klimenko et al. 2005, 2006), and a ringdown templated search (Aasi et al. 2014). Improvement in the detector sensitivity at low frequencies in the advanced era made IMBH binaries a target for a matched filtering search that would probe the short inspiral phase. In Abbott et al. (2017b), we used a combined search with the matched filtering GstLAL (Messick et al. 2017; Hanna et al. 2020; Sachdev et al. 2019) search and model independent cWB (Klimenko et al. 2011, 2016). This combined search was further extended with an additional matched filtering PyCBC search (Usman et al. 2016; Allen 2005; Dal Canton et al. 2014; Nitz et al. 2017) in Abbott et al. (2019) using the data from the first two observing runs. No significant IMBH binary event was found in these searches.

While all the previous matched filtering searches were generic BBH searches, the improvements in the detector sensitivity at low frequencies and the IMBH merger signals' short duration nature motivated us to use matched filter searches targeted to the IMBH mass-spin parameter space. Here, we carry out an IMBH binary search using the entire year-long third observing run, O3, of the Advanced LIGO and Advanced Virgo detector network with a combined search using three search algorithms: two matched-filtering based focused IMBH binary searches, using the PyCBC and GstLAL libraries, and the minimally modelled time-frequency based cWB search. We search for massive binary systems with at least one component above the expected PISN mass gap limit of $65\,\mathrm{M}_\odot$, and with an IMBH remnant. GW190521 remains as the most significant candidate in the combined search; no other event is comparably significant. We provide the results from the combined search with the next most significant events and follow up investigations to assess their origin.

The increased sensitivity of the O3 run allows us to set more stringent bounds on the binary merger rate density. The lack of a confirmed IMBH population as well as possible formation channels of IMBH distinct from those of stellar-mass BHs preclude us from using an overall mass model for the IMBH population. Thus, we confine all the upper limit studies to a suite of discrete points in the IMBH parameter space. We incorporate more detailed physics in selecting the suite of IMBH binary waveforms as compared to earlier upper limit studies. In Abbott et al. (2017b) we simulated a limited set of discrete mass and aligned-spin binary waveforms in the first advanced detector observation data to obtain upper limits on merger rate. The study with the first two observation runs used the most realistic numerical relativity (NR) simulation set with aligned spins for the upper limit study (Abbott et al. 2019). The most recent stringent merger rate

[1] The parameter estimated values for GW190521 reported in GWTC-2 are slightly different from that of the detection paper. The estimation in the detection paper is based on the NRSur7dq4 waveform model, and GWTC-2 values are obtained from the estimates averaged over three waveforms; SEOBNRv4PHM, NRSur7dq4, and IMRPhenomPv3HM, respectively.

upper limit is 0.2 $\mathrm{Gpc^{-3}yr^{-1}}$, for the equal mass binary system with a component mass of 100 $M_\odot$ and component spins of dimensionless magnitude 0.8 aligned with the binary orbital angular momentum. Recently, Chandra et al. (2020) used IMBH binary systems with generically spinning BHs with total mass between 210 – 500 $M_\odot$ and obtained a most stringent upper limit of 0.28 $\mathrm{Gpc^{-3}yr^{-1}}$ for equal-mass binaries with total mass of 210 $M_\odot$.

Here, we use a suite of NR simulations of GW emission from IMBH binary system with generically spinning BHs in order to estimate our search sensitivity over the O3 data. We place the most stringent 90% merger rate upper limit on equal mass and aligned spin BH binary of total mass 200 $M_\odot$ and with individual BH spins of 0.8 as 0.056 $\mathrm{Gpc^{-3}yr^{-1}}$. The revised limit is a factor $\sim$ 3.5 more stringent than that obtained with the first two observing runs. We also update the merger rate for systems compatible with the source parameters of GW190521, first estimated in Abbott et al. (2020c), to $0.08^{+0.19}_{-0.07}$ $\mathrm{Gpc^{-3}yr^{-1}}$, using the combined search method applied to simulated signals injected over the entire O3 data.

The paper organization is as follows: Sect. 2 summarizes the data being used for the search. Sect. 3 summarizes the combined search approach from the results from three distinct IMBH binary search algorithms. Sect. 4 discusses the search results and followup of the most significant candidate events. Sect. 5 provides a detailed discussion about the NR GW injection set used and the rate upper limits study including the updated rate on the most significant GW190521-like systems.

2. Data Summary

We carry out the analysis using O3 data from both LIGO detectors (LHO-LIGO Hanford Observatory and LLO-LIGO Livingston Observatory) and the Virgo detector. We condition the data in multiple steps before performing our search (Abbott et al. 2020a). The strain data, recorded from each detector, are calibrated in near real-time to produce an online data set (Viets et al. 2018; Acernese et al. 2018). A higher-latency offline calibration stage provides identification of systematic errors and calibration configuration changes (Sun et al. 2020; Estevez et al. 2020). The analyses presented here use the offline recalibrated data from the LIGO detectors, and the Virgo detector's online data. For this search, we consider 246.2 days, 254.1 days, and 250.8 days of observing-mode data from the Hanford, Livingston, and Virgo detector respectively. The joint observation time for the full network of three detectors is 156.4 days.

We then linearly subtract spectral features of known instrumental origin using auxiliary witness sensors, i.e., sensors that indicate the presence of noise causing these features. The subtraction removes calibration lines in all detectors, as well as 60 Hz harmonics produced by power mains coupling in the LIGO detectors (Driggers et al. 2019; Davis et al. 2019). Low-frequency modulation of the power mains coupling also results in sidebands around the 60 Hz line; we apply an additional non-linear noise subtraction to remove these sidebands (Vajente et al. 2020).

Periods of poor data quality are marked using data quality flags separated into three categories (Abbott et al. 2020a; Fisher et al. 2020; Davis et al. 2021), which are used to exclude time segments from different searches, as described below. Category 1 flags indicate times when a detector is not operating or recording data in its nominal state; these periods are not analyzed by any search. Category 2 flags indicate periods of excess noise that are highly likely to be caused by known instrumental effects. The cWB and PyCBC searches use different sets of category 2 flags. The GstLAL search does not use category 2 flags, as discussed in Sect. 3. Category 3 flags are based on statistical correlations with auxiliary sensors. Of the analyses presented here, only the cWB search uses category 3 flags.

The candidate events in this paper are vetted in the same way as past GW events (Abbott et al. 2016a, 2021a). This validation procedure identifies data quality issues such as non-stationary noise or glitches of instrumental origin appearing in the strain data. Auxiliary sensors that monitor the detectors and environmental noise are used to check for artifacts that may either have accounted for, or contaminated the candidate signal (Nguyen et al. 2021). For candidate events that coincide with glitches, subtraction of the glitches from the strain data is performed if possible (Cornish & Littenberg 2015; Littenberg et al. 2016; Pankow et al. 2018); otherwise recommendations are made to exclude the relevant time or frequency ranges from parameter estimation analyses. Validation assessments for individual candidate events are provided in Sect.4 and Appendix A.

3. Search methods

In this section, we describe the analysis methods algorithms (pipelines) used to search the LIGO-Virgo data from O3 for IMBH binary merger signals. Such signals have short durations in the detectors' sensitive frequency band, typically less than 1 s. Thus, methods for detection of generic short transient GW events (bursts) may be competitive compared to search methods which use parameterized models of the expected signals (templates) from binary coalescences (e.g. Chandra et al. 2020). As in the IMBH binary search of O1 and O2 (Abbott et al. 2017b, 2019), we employ both generic transient search methods and modelled template searches. We first describe the generic transient pipeline, cWB, in the configuration used here, and then the two templated pipelines, GstLAL and PyCBC, which have been adapted to maximize sensitivity to IMBH binary mergers. We then summarize the method used to combine the search outputs into a single candidate list, and finally discuss selection criteria to distinguish IMBH binary candidates from the known heavy stellar-mass BBH population (Abbott et al. 2021a,c).

The output of a transient search algorithm or pipeline is a set of candidate events, each with an estimated time of peak strain at the participating detector(s).[2] Each event is also assigned a ranking statistic value, and its significance is quantified by estimating the corresponding false alarm rate (FAR), which is the expected number per time of events caused by detector noise that have an equal or higher ranking statistic value.

The sensitivity of a search to a population of IMBH mergers can be evaluated by adding simulated signals (injections) to real GW detector strain data and analyzing the resulting data streams, to output the ranking statistic and estimated FAR that each simulated signal would be assigned if present in an actual search. Specific simulation campaigns will be described in detail in Sect. 5 and sensitivity estimates from individual search pipelines are included in a public data release.

3.1. cWB model waveform independent search for IMBH binaries

cWB (Klimenko & Mitselmakher 2004; Klimenko et al. 2005, 2006, 2011, 2016; Drago et al. 2020) is a GW search that uses

[2] For black hole binary mergers, this peak strain time is close to the formation of a common horizon.

minimal assumptions on signal morphology to detect and reconstruct GW transients. The search identifies coincident energy across the network of detectors to classify GW signals. The cWB search has been participating in the search for IMBH signals since Initial LIGO's fifth science run (Abadie et al. 2012a). The algorithm uses a multi-resolution wavelet transform, known as the Wilson Daubechies Meyer wavelet transform (Necula et al. 2012), to map the multi-detector data into the time-frequency domain, as blocks of a fixed time-frequency area known as pixels. The algorithm selects pixels with excess energy above the expected noise fluctuation and groups them into clusters, referred to as candidate events. The collection and clustering of pixels differ based on the target source (Klimenko et al. 2016). Each candidate event is ranked according to its coherent signal-to-noise ratio (SNR) statistic (Klimenko et al. 2016), which incorporates the estimated coherent energy and residual noise energy. An additional threshold is applied to the network correlation which provides the measure on the event correlation across multiple detectors in the network. The cWB algorithm reconstructs the source sky location and whitened signal waveforms using the constrained maximum likelihood method (Klimenko et al. 2016).

We estimate the FAR of a search event with time lag analysis: data from one or more detectors are time-shifted by more than 1 s with respect to other detectors in the network, then cWB identifies events in this time-shifted data. Since the time-shift is greater than the GW time of flight between detectors, this analysis estimates the rate and distribution of false alarms. The analysis is repeated many times with different time-shifts, yielding a total analyzed background time $T_{\rm bkg}$. For a given search event, the FAR value is estimated as the number of background events with coherent SNR greater than the value assigned to the event, divided by $T_{\rm bkg}$.

The model independent nature of cWB search makes it susceptible to incorrectly classifying noise artifacts. We apply a series of signal-dependent vetoes based on the time-frequency morphology and energy distribution properties to remove spurious noisy transients. We tune the veto values based on the extensive simulation of IMBH binary signals (see Appendix A of Gayathri et al. 2019). We divide the cWB search for quasi-circular BBH signals into two separate configurations: high-mass search and low-mass search, depending on the central frequency $f_{\rm c}$ of the GW signal. For a compact binary merger signal, $f_{\rm c}$ is inversely proportional to the redshifted total mass $M_z = (1+z)M$, where M is the source frame total mass and z is the source redshift. We then optimize the low-mass search sensitivity for signals with $f_{\rm c} > 80\,$Hz (the BBH regime), and the high-mass search sensitivity for signals with $f_{\rm c} < 80\,$Hz (the IMBH regime). In practice, a cut $f_{\rm c} > 60\,$Hz is imposed in the low-mass search and $f_{\rm c} < 100\,$Hz in the high-mass search, resulting in an overlap region covering $60-100\,$Hz. In the O3 search, we combine the two searches by applying a trials factor of 2 to the estimated FAR for events in the overlap region. This improves the overall search sensitivity to borderline IMBH events (Szczepańczyk et al. 2021).

The cWB search analyzes data from all three detectors in low latency. However, the follow up offline cWB analysis does not improve detection efficiency with the inclusion of Virgo. This is primarily due to the additional noise in the Virgo detector. Thus, at a given time, the cWB search uses the best available (most sensitive) two detector network configuration. This ensures that the cWB search does not analyze the same data with multiple detector configurations. In case, if any event shows high significance in low latency cWB analysis with the three-detector network and low significance in offline cWB analysis with the best two-detector configuration, we re-analyze that observing time with both the LLO-LHO-Virgo and LLO-LHO networks and apply a trials factor of 2 to the minimum FAR over the two networks for the final significance.

3.2. Templated searches for IMBH mergers

For GW signals whose forms are known or can be theoretically predicted, search sensitivity is optimized by the use of matched filter templates that suppress noise realizations inconsistent with the predicted signals. Since the binary parameters are *a priori* unknown, a discrete set (bank) of templates is used in order to cover signal parameter values within a predetermined range with a specified minimum waveform accuracy (Sathyaprakash & Dhurandhar 1991; Owen 1996). General binary black hole coalescence signals bear the imprint of component spins misaligned with the orbital axis, causing orbital precession, and potentially also of orbital eccentricity. It is a so far unsolved problem to implement an optimal search over such a complex space of signals.

Instead, the searches presented here restrict the signal model to the dominant mode of GW emission from quasi-circular, non-precessing binaries (Ajith et al. 2011), i.e. with component spins perpendicular to the orbital plane. Both the GstLAL and PyCBC searches use the SEOBNRv4 waveform approximant (Bohé et al. 2017) as template waveforms, implemented as a reduced-order model (Pürrer 2016) for computational speed. These templates may still have high matches to signals from precessing or eccentric binaries, however in general, sensitivity to such signals will be reduced due to lower matches with template waveforms.

Each detector's strain time series is then correlated with each template to produce a matched filter time series. Single-detector candidates are generated by identifying maxima of the matched filter SNR above a predetermined threshold value. However, during times of known disturbances in detector operation, or during very high amplitude non-Gaussian excursions in the strain data, candidates are either not produced or are discarded, since such high-SNR maxima are very likely to be artifacts. Signal consistency checks such as chi-squared (Allen 2005) are also calculated and single-detector candidates may also be discarded for excessive deviation from the expected range of values.

If two or more detectors are operating, their single-detector candidates are compared in order to identify multi-detector candidate events which are consistent in the template parameters, time of arrival, amplitude, and waveform phase over the detector network. The resulting multi-detector events are then ranked via a statistic which depends on the properties of single-detector candidates and their consistency over the network. Finally, the statistical significance of each multi-detector event is obtained by comparing its statistic value to the distribution expected for noise events, resulting in an estimate of its FAR.

In what follows we briefly summarize the methods specific to each of the matched filter pipelines.

3.2.1. GstLAL search

The search for IMBH mergers executed by the matched filter based GstLAL pipeline (Messick et al. 2017; Hanna et al. 2020; Sachdev et al. 2019; Cannon et al. 2021) uses a template bank covering a parameter space of binaries with (redshifted) total masses in the range $[50, 600]\,\mathrm{M}_{\odot}$. The mass ratios, $q = m_2/m_1$, of the binary systems covered lie between 1 and $1/10$, while their spins are either aligned or anti-aligned with the total angular momentum of the system, with the dimensionless spin magnitude less than 0.98. The analysis starts at a frequency of 10 Hz.

The SNR threshold applied for single-detector triggers is 4 for the Hanford and Livingston detectors and 3.5 for the Virgo detector. The GstLAL search pipeline applies a signal-consistency test based on the template's autocorrelation over time. The search also uses a signal model to describe the prior probability of a binary from a given source population being detected by each template: the signal model used for this search is uniform in the log of the reduced mass of the binary.

The ranking statistic applied to candidate events is an estimate of the relative probability of the event's parameters being caused by a GW signal as compared to noise, i.e. the likelihood ratio. In addition to events formed from triggers from multiple detectors, triggers found in a single detector are also included in the search, albeit with a penalty applied to their ranking to account for the higher probability of noise origin.

The GstLAL search does not use data quality based vetoes of category 2 and above. Instead, the search uses data quality information known as iDQ (Essick et al. 2020; Godwin et al. 2020), from auxiliary channels monitoring the detector to compute a penalty term in the denominator of the ranking statistic. This has been computed for both single-detector and multi-detector triggers found by the search. The non-coincident and noise-like triggers are then used to estimate the background noise probability density, which is sampled to find the estimated FAR, corresponding to the likelihood ratio for a candidate (Messick et al. 2017; Sachdev et al. 2019).

3.2.2. PyCBC search

The PyCBC-IMBH search used here (Chandra et al. 2021) covers a target space of redshifted total masses between 100 and 600 $M_\odot$, with component masses greater than 40 $M_\odot$ and mass ratio between 1/1 and 1/10. The components have dimensionless spins projected onto the orbital axis between −0.998 and 0.998. To reduce false alarms arising from short-duration noise transients (Cabero et al. 2019), we discard any templates with a duration less than 0.07 s, measured from the fixed starting frequency of 15 Hz.

The analysis pre-processes the data from each detector by windowing out very high amplitude excursions ($> 50\sigma$ deviation from Gaussian noise) in the whitened strain time-series (Usman et al. 2016). This gating step significantly suppresses the noise background. The SNR threshold for trigger generation is chosen as 4; any triggers in time marked by category-2 data quality veto are discarded. We also remove LIGO triggers within $(-1, +2.5)$ s of the centre of a gating window, since empirically such times contain many lower-amplitude noise transients correlated with the central high amplitude glitch (Chandra et al. 2021).

Signal-consistency χ_r^2 and sine-Gaussian discriminant tests are applied to the remaining triggers (Allen 2005; Nitz 2018). The single detector SNRs are corrected for short-term variation in the detector power spectral density (PSD) (Nitz et al. 2019; Mozzon et al. 2020), and a penalty is applied to triggers with a short-term PSD measure over 10 times the expectation from stationary noise (Chandra et al. 2021). The analysis also penalizes triggers with χ_r^2 values above 10, where the expectation for a well-matched signal is unity. These vetoes significantly reduce the background.

The search identifies candidates by checking the consistency between triggers in 2 or 3 detectors. The resulting candidates are ranked by using the expected distribution of astrophysical signal SNRs, phases and times over multiple detectors, as well as models of the non-Gaussian noise distribution in each template and detector (Nitz et al. 2017; Davies et al. 2020). A FAR is assigned to each candidate event by simulating the background noise distribution using time-shifted analyses (Usman et al. 2016), similar to cWB. The FARs for events involving different detector combinations are finally combined as in Davies et al. (2020).

Other PyCBC-based searches overlapping the IMBH parameter region were recently presented in Nitz et al. (2019) and Abbott et al. (2021a) using two strategies: a broad parameter space search covering compact binaries from binary neutron star (BNS) up to IMBH, and a "focused" search for binary black hole (BBH) covering a restricted range of masses and with strict cuts to suppress noise artifacts. The sensitivity of the present IMBH search, at a FAR threshold of 0.01 yr^{-1}, to a set of simulated generically spinning binary merger signals is increased relative to the broad (BBH) PyCBC searches of Abbott et al. (2021a) by a factor of ~ 1.5 (~ 1.1) in volume time (VT) for redshifted total mass $M_z \in [100-200]\,\mathrm{M}_\odot$, up to a factor ~ 2.8 (~ 12.6) for $M_z \in [450, 600]\,\mathrm{M}_\odot$ (Chandra et al. 2021).

3.3. Combined search

Each of our three targeted searches produces its list of candidates characterized by GPS times and FAR values. The p-value for each candidate in a given search, defined as the probability of observing one or more events from the noise alone with a detection statistic as high as that of the candidate is then

$$p = 1 - e^{-T\cdot\mathrm{FAR}}, \tag{1}$$

where T is the total duration of data analyzed by the search. We combine these lists to form a single list of candidates by first checking whether any events from different searches fall within a 0.1s time window of each other, and if so, selecting only the event with the lowest p-value $p_{\min}$. The resulting clustered events are ranked by a combined p-value,

$$\bar{p} \equiv 1 - (1 - p_{\min})^m, \tag{2}$$

where m denotes the trials factor (look-elsewhere) factor (Abbott et al. 2017b, 2019). We take $m = 3$ under the assumption that the noise backgrounds of our searches are independent of one another. If there is any correlation between these backgrounds, the effective trials factor will be lower, which makes $m = 3$ a conservative choice.

3.4. Selection of Intermediate Mass Black hole Binaries

As noted in Abbott et al. (2021a,c), LIGO-Virgo observations include a population of black hole binaries with component masses extending up to 60 $\mathrm{M}_\odot$ or above, and remnant masses extending up to $\sim$ 100 $\mathrm{M}_\odot$; thus, there is *a priori* no clear separation between such heavy BBH systems and the lightest IMBH binaries. We also expect search pipelines tuned for sensitivity to IMBH mergers to be capable of detecting such heavy stellar-mass BBH, since the overlap of their GW signals with those of IMBH binaries may be large. We find indeed that many such BBH systems occurring within O3a are recovered with high significance by our search.

Here, we select only those events for which, under the assumption that the signals were produced by a quasi-circular binary black hole merger, we have clear evidence that the remnant is an IMBH of mass above 100 $\mathrm{M}_\odot$, and at least the primary black hole has a mass greater than the lower bound of the pair-instability mass gap, for which we take a conservative estimate under the standard assumptions on the $^{12}C(\alpha,\gamma)^{16}O$ reaction rate etc. to be, $m_1^* = 65 M_\odot$ (see e.g. Woosley 2017,Stevenson et al. 2019, Belczynski et al. 2020, Costa et al. 2021, Tanikawa et al. 2021, Vink et al. 2021). Strong evidence that this is the case for the primary component of GW190521 was presented in Abbott et al. (2020b,c). Furthermore, the maximum component mass of the black hole binary population seen up to O3a is confidently above $\sim 50\,M_\odot$ even if GW190521 is excluded from the analysis (see Fig. 2 of Abbott et al. 2021c); thus, we place a more stringent condition on the primary mass to identify potential outliers from this population.

The selection criteria are evaluated as follows. We begin by defining the hypothesis H according to which the detector output time series $d(t)$ is given by

$$d(t) = n(t) + h(t;\theta) \tag{3}$$

where $n(t)$ is the noise time series, taken as a realisation of a zero-mean wide-sense stationary stochastic process, and $h(t;\theta)$ is the gravitational wave signal model dependent on a set of parameters θ. We estimate the parameters θ by computing their posterior probability distribution $p(\theta|d,H)$ using Bayes theorem:

$$p(\theta|d,H) = p(\theta|H)\frac{p(d|\theta,H)}{p(d|H)} \tag{4}$$

where $p(\theta|H)$ is the prior probability distribution, $p(d|\theta,H)$ is the likelihood function – taken as Normal distribution in the frequency domain with variance given by the power spectral density of the data $d(t)$ thanks to the wide-sense stationarity assumption – and

$$p(d|H) = \int d\theta\, p(\theta|H)p(d|\theta,H) \tag{5}$$

is the *evidence* for the hypothesis H.

Each potential candidate is followed up with a coherent Bayesian parameter estimation analysis (Veitch et al. 2015; Lange et al. 2017; Wysocki et al. 2019). In these analyses, we model the GW signal as represented by precessing quasi-circular waveforms from three different families: `NRSur7dq4` (Varma et al. 2019), `SEOBNRv4PHM` (Ossokine et al. 2020) and `IMRPhenomXPHM` (Pratten et al. 2021). All considered models include the effects of higher-order multipole moments as well as orbital precession due to misaligned BH spins. Details of the analysis configuration follow previously published ones (Abbott et al. 2021a) and are documented in a separate paper (Abbott et al. 2021b). In particular, we consider uniform priors on the redshifted component masses, the individual spin magnitudes, and the luminosity distance proportional to its square modulus. For the source orientation and spin vectors, we employ isotropic priors.

As a quantitative criterion to select a GW event as an IMBH binary, we consider the support of the joint posterior distributions for the primary mass m_1 and of the remnant mass M_f. For reference values $M^* = 100 M_\odot$ and $m_1^* = 65 M_\odot$, we label a candidate an intermediate-mass black hole binary if

$$\int_{M^*}^{+\infty}\int_{m_1^*}^{+\infty} dm_1\, dM_f\, p(M_f, m_1|d,H) \geq p^*, \tag{6}$$

where p^* is a reference probability threshold, chosen to be $p^* = 0.9$. To perform the integral in Eq. (6), we construct a Gaussian kernel density estimate to interpolate the posterior $p(M_f, m_1|d,H)$ which we use to perform the integral on a grid.

Thus, the main list of candidates presented in the following section does not correspond to the complete set of events recovered by the searches, but only to those relevant to a potential astrophysical IMBH population. However, for comparison with earlier results (Abbott et al. 2021a), we also report a full list of events detected by the combined IMBH search in O3a data, including BBH events that do not fall into the IMBH region: see Sect. 4.2. A catalog of confidently detected heavy BBH systems over the complete O3 run will be provided in a subsequent publication, as an update to GWTC-2.

The data for some events may not be consistent with the quasi-circular BBH signal plus Gaussian noise model, either because they contain a signal which deviates significantly from this standard BBH model, or are affected by detector noise artefacts that cannot be removed or mitigated. In such cases the values of $p(M_f|d,H)$ and $p(m_1|d,H)$ extracted from the Bayesian analysis may either be inaccurate or indeed meaningless, for events arising from instrumental noise or even from a putative astrophysical source that is not a compact binary merger. Such events will *not* be excluded from results presented here: they will be individually discussed in the following sections.

4. Search results

4.1. Candidate IMBH events

The individual searches are applied on the full O3 data with the analysis time of 0.734 yr, 0.747 yr and 0.874 yr for cWB, PyCBC-IMBH and GstLAL-IMBH search respectively.

In Table 1 we report events satisfying the criteria for potential IMBH binaries in Sect.3, in increasing order of combined p-value (see Eq.3), up to and including the most significant event with unambiguous evidence of instrumental noise origin, 200214_224526. For completeness, we have also listed marginal triggers found by our combined search in Appendix A.

The top-ranked event is GW190521 and it has a highly significant combined p-value of 4.5×10^{-4}. If this signal is from a quasi-circular merger, then the signal is found to be consistent with the merger of two black holes in a mildly precessing orbit, with component masses of $85^{+21}_{-14}\,M_\odot$ and $66^{+17}_{-18}\,M_\odot$ and a remnant black hole of $142^{+28}_{-16}\,M_\odot$ falling in the mass range of intermediate-mass black holes. A full description of GW190521 and its implications can be found in Abbott et al. (2020b,c).

The second-ranked candidate, 200114_020818, was observed on 14th January 2020 at 02:08:18 UTC and identified by the low latency cWB search in the LHO-LLO-Virgo detector network configuration, with a FAR of $< 0.04\,\mathrm{yr}^{-1}$. The event was publicly reported via GCN minutes after the event was observed (Abbott, R. and others 2019). Given the significance of the low-latency alert with the 3-detector configuration, we employ both LHO-LLO and LHO-LLO-Virgo networks in cWB to estimate the significance for this event: we find FARs of $15.87\,\mathrm{yr}^{-1}$ and $0.029\,\mathrm{yr}^{-1}$ for these configurations, respectively. The SNR reconstructed by cWB for each network configuration is 12.3 and 14.5, respectively. As mentioned above in 3.1, we apply a trials factor of 2 to the most significant result, obtaining a FAR of $0.058\,\mathrm{yr}^{-1}$ for the cWB search. The combined p-value of this event, 0.12, is marginally significant.

We then examined possible environmental or instrumental causes for the candidate signal. Excess vibrational noise could have contributed to the signal in the LIGO Hanford detector, as discussed in Appendix B.1. Furthermore, the morphology

Events	GPS Time	cWB FAR (yr^{-1})	PyCBC FAR (yr^{-1})	GstLAL FAR (yr^{-1})	$\bar{p}$
GW190521	1242442967.5	2.0×10^{-4}	1.4×10^{-3}	1.9×10^{-3}	4.5×10^{-4}
200114_020818 †	1263002916.2	5.8×10^{-2}	$8.6 \times 10^{+2}$	$3.6 \times 10^{+4}$	1.2×10^{-1}
200214_224526	1265755544.5	1.3×10^{-1}	-	-	2.5×10^{-1}

Table 1. Events from the combined search for intermediate mass black hole binary mergers in O3 data, sorted by their combined p-value $\bar{p}$. † 200114_020818 was recovered by the cWB search using LHO-LLO data with a FAR of 15.87 yr^{-1} and by a followup search using LHO-LLO-Virgo data with a FAR of 0.029 yr^{-1}; the FAR quoted in the table for cWB is derived from the LHO-LLO-Virgo search with a trials factor of 2.

of 200114_020818 is consistent with a well-studied class of glitches known as Tomtes (Buikema et al. 2020; Davis et al. 2021), which occur multiple times per hour in LIGO Livingston. However, we are not currently able to exclude a putative morphologically similar astrophysical signal, as there are no known instrumental auxiliary channels that couple to this glitch type. We undertake detailed model-independent event reconstruction and parameter estimation (PE) studies, summarized in Appendix B. Although model independent methods/algorithms produce mutually consistent reconstructions of the event, our analysis using the available quasi-circular BBH merger waveforms does not support a consistent interpretation of the event as a binary merger signal present across the detector network. We cannot conclusively rule out an astrophysical origin for the event, however it also appears consistent with an instrumental artefact in LLO in coincidence with noise fluctuations in LHO and Virgo.

The third-ranked event was observed by the cWB pipeline on 14th February, 2020 at 22:45:26 UTC with a combined SNR of 13.1 in the two Advanced LIGO Detectors. The event has a $p_{\mathrm{cWB}} = 0.092$ and thus a $\bar{p} = 0.251$. In addition to its marginal significance, the event has characteristics consistent with an instrumental noise transient. Excess noise due to fast scattered light (Soni et al. 2021) is present in both LLO and LHO data. At Livingston, the excess noise extends up to 70 Hz and lasts many seconds before and after the event. The Hanford scattering noise is weaker in amplitude but still overlaps completely with the duration of the event. Since it is the most significant noise event obtained in the combined search with the cWB pipeline in its production configuration considering only 2-detector events, we use 200214_224526 to establish a threshold of significance for inference of IMBH merger rates (for which see Sect. 5). As 200214_224526 is likely caused by detector noise, any events with lower significance may be assumed to have a high probability of noise origin. For completeness, we discuss some marginal events from the combined search in Appendix A.

4.2. Complete O3a search results including BBH

As noted earlier in 3, the template-based searches have high sensitivity to the known population of heavy stellar-mass BBH mergers, which may be compared to searches deployed in GWTC-2 (Abbott et al. 2021a). Here we record the complete list of significant events recovered by the combined IMBH search from O3a data in Table 2, and supply corresponding search results from GWTC-2 for comparison. Specifically, we show outputs from the PyCBC broad parameter space and focused BBH searches (Nitz et al. 2019) and the GstLAL broad parameter space search (Sachdev et al. 2019).

For GW190521, the PyCBC IMBH search yields a FAR of $1.4 \times 10^{-3}\,yr^{-1}$, as compared to 1.1 yr^{-1} for the broad parameter space analysis of Abbott et al. (2020b, 2021a). This significant change is in part because the PyCBC IMBH search is optimized for shorter duration signals, and does not consider potential signals of total mass significantly below 100 $M_{\odot}$; the mass and spin values of GW190521 are also likely not covered by the templates used in earlier PyCBC searches, which imposed a minimum duration of 0.15 s. A similar change in statistical significance is also observed for GW190602_175927 for the same reasons. However, the IMBH search results assign lower significance to GW190519_153544 and GW190706_222641 as compared to the GWTC-2 results.

The GstLAL pipeline recovers the GW190521 event at a FAR of $1.9 \times 10^{-3}\,yr^{-1}$ over all of O3 data. It was reported earlier (Abbott et al. 2020b, 2021a) at a FAR of $1.2 \times 10^{-3}\,yr^{-1}$ over O3a. As described in 3.2.1, the GstLAL pipeline has employed a dedicated search for IMBH binaries with better coverage for the heavier mass binaries than the catalog search. Also, the iDQ based data quality information used to inform the calculation of the ranking statistics, now incorporates multi-detector triggers, as against the only single detector triggers that were used before. Differences in the significance of the events found by the IMBH specific GstLAL search presented here, with what was reported for O3a in Abbott et al. (2021a) can be attributed to the differences in the search settings and the data spanning over all of O3.

5. Astrophysical Rates of IMBH Binary Coalescence

Improved detector sensitivity, updated search methods, and the detection of GW190521 allow us to obtain revised bounds on the merger rate (strictly, rate density) of IMBH binaries. Due to the lack of knowledge of specific formation channels for IMBH binaries, even more so than for stellar-mass BH binaries, and the sparse observational evidence of any IMBH population, we do not consider any overall mass model for such a population. Instead, here we simulate a suite of IMBH binary waveforms for discrete points in parameter space, including generically spinning component BHs, derived from NR simulations. A similar campaign was carried out in Abbott et al. (2019) using NR waveforms for IMBH binaries having component BH spins aligned with the binary orbital axis, injected into the O1 and O2 data.

5.1. Injection Set

Here, we report on the merger rate of IMBH binary sources based on NR simulations computed by the SXS (Mroué et al. 2013), RIT (Healy et al. 2017), and GeorgiaTech (Jani et al. 2016) codes. These simulations include higher-order multipoles, which may make important contributions to the detection of high-mass and low mass-ratio ($q \leq 1/4$) binaries (Calderón Bustillo et al. 2016). Based on previous studies which measured the agreement between different NR codes (Abbott et al. 2019), we in-

Event	cWB	PyCBC			GstLAL		Combined
		GWTC-2 Broad	GWTC-2 BBH	IMBH	GWTC-2 Broad	IMBH	IMBH
	FAR (yr^{-1})	FAR (yr^{-1})			FAR (yr^{-1})		$\bar{p}$
GW190408_181802	9.5×10^{-4}	$< 2.5 \times 10^{-5}$	$< 7.9 \times 10^{-5}$	1.6×10^{-2}	$< 1.0 \times 10^{-5}$	$< 1.0 \times 10^{-5}$	$< 1.0 \times 10^{-4}$
GW190413_052954	-	-	7.2×10^{-2}	5.6×10^{-1}	-	$5.4 \times 10^{+3}$	7.1×10^{-1}
GW190413_134308	-	-	4.4×10^{-2}	1.4×10^{-1}	3.8×10^{-1}	$1.2 \times 10^{+3}$	2.7×10^{-1}
GW190421_213856	3.0×10^{-1}	$1.9 \times 10^{+0}$	6.6×10^{-3}	6.1×10^{-3}	7.7×10^{-4}	$1.8 \times 10^{+0}$	1.4×10^{-2}
GW190503_185404	1.8×10^{-3}	3.7×10^{-2}	$< 7.9 \times 10^{-5}$	2.5×10^{-3}	$< 1.0 \times 10^{-5}$	1.7×10^{-1}	4.0×10^{-3}
GW190512_180714	8.8×10^{-3}	3.8×10^{-5}	$< 5.7 \times 10^{-5}$	$4.0 \times 10^{+1}$	$< 1.0 \times 10^{-5}$	$< 1.0 \times 10^{-5}$	$< 1.0 \times 10^{-4}$
GW190513_205428	-	3.7×10^{-4}	$< 5.7 \times 10^{-5}$	5.0×10^{-2}	$< 1.0 \times 10^{-5}$	2.1×10^{-1}	1.1×10^{-1}
GW190514_065416	-	-	5.3×10^{-1}	$1.1 \times 10^{+0}$	-	$7.6 \times 10^{+2}$	9.2×10^{-1}
GW190517_055101	8.0×10^{-3}	1.8×10^{-2}	$< 5.7 \times 10^{-5}$	8.7×10^{-4}	9.6×10^{-4}	2.7×10^{-2}	1.9×10^{-3}
GW190519_153544	3.1×10^{-4}	$< 1.8 \times 10^{-5}$	$< 5.7 \times 10^{-5}$	$< 1.1 \times 10^{-4}$	$< 1.0 \times 10^{-5}$	3.9×10^{-3}	2.5×10^{-4}
GW190521	2.0×10^{-4}	$1.1 \times 10^{+0}$	-	1.4×10^{-3}	1.2×10^{-3}	1.9×10^{-3}	4.5×10^{-4}
GW190521_074359	$< 1.0 \times 10^{-4}$	$< 1.8 \times 10^{-5}$	$< 5.7 \times 10^{-5}$	$< 2.3 \times 10^{-5}$	$< 1.0 \times 10^{-5}$	$< 1.0 \times 10^{-5}$	$< 1.0 \times 10^{-4}$
GW190602_175927	1.5×10^{-2}	-	1.5×10^{-2}	1.1×10^{-3}	1.1×10^{-5}	$< 1.0 \times 10^{-5}$	$< 1.0 \times 10^{-4}$
GW190701_203306	3.2×10^{-1}	-	-	$< 1.9 \times 10^{-4}$	1.1×10^{-2}	3.8×10^{-2}	4.3×10^{-4}
GW190706_222641	$< 1.0 \times 10^{-3}$	6.7×10^{-5}	4.6×10^{-5}	$< 1.1 \times 10^{-4}$	$< 1.0 \times 10^{-5}$	2.4×10^{-3}	2.5×10^{-4}
GW190727_060333	8.8×10^{-2}	3.5×10^{-5}	3.7×10^{-5}	$< 1.2 \times 10^{-4}$	$< 1.0 \times 10^{-5}$	4.5×10^{-4}	2.7×10^{-4}
GW190731_140936	-	-	2.8×10^{-1}	6.4×10^{-1}	2.1×10^{-1}	$2.1 \times 10^{+0}$	7.6×10^{-1}
GW190803_022701	-	-	2.7×10^{-2}	1.7×10^{-1}	3.2×10^{-2}	$3.0 \times 10^{+0}$	3.2×10^{-1}
GW190828_063405	$< 9.6 \times 10^{-4}$	$< 1.0 \times 10^{-5}$	$< 3.3 \times 10^{-5}$	$< 7.0 \times 10^{-5}$	$< 1.0 \times 10^{-5}$	$< 1.0 \times 10^{-5}$	$< 1.0 \times 10^{-4}$
GW190915_235702	$< 1.0 \times 10^{-4}$	8.6×10^{-4}	$< 3.3 \times 10^{-5}$	3.8×10^{-4}	$< 1.0 \times 10^{-5}$	4.7×10^{-1}	2.2×10^{-4}
GW190929_012149	-	-	-	3.1×10^{-1}	2.0×10^{-2}	$2.9 \times 10^{+1}$	5.0×10^{-1}

Table 2. Candidate events from this search for IMBH mergers in O3a data, including binary black hole mergers outside the IMBH parameter space, and comparison with previously obtained GWTC-2 results from the templated search algorithms (Abbott et al. 2021a). The cWB search algorithm used here is unchanged over GWTC-2. Candidates are sorted by GPS time and the FAR is provided for each search algorithm. Templated methods used in GWTC-2 comprise the PyCBC and GstLAL broad parameter space pipelines and the PyCBC BBH-focused pipeline, while the optimized algorithms applied in this search are labelled "IMBH". The event names encode the UTC date with the time of the event given after the underscore, except for the individually published event GW190521. The GstLAL FAR values have been capped at $1.0 \times 10^{-5}\ \mathrm{yr}^{-1}$ and corresponding $\bar{p}$ values have also been capped. For PyCBC events with FAR estimates limited by finite background statistics, an upper limit is stated. The IMBH combined search p-values $\bar{p}$ for each event are calculated from Eq. (6) using p-values of the cWB, PyCBC-IMBH and GstLAL-IMBH searches.For details of the search configurations and event parameters, refer to Abbott et al. (2021a).

clude the following harmonic modes in our analysis: $(\ell, m) = \{(2, \pm1), (2, \pm2), (3, \pm2), (3, \pm3), (4, \pm2), (4, \pm3), (4, \pm4)\}$.

We consider 43 IMBH binary sources with fixed source frame masses and spins, shown in Table 3. These 43 sources include a subset of 16 sources investigated in the O1-O2 IMBH binary search. This updated search includes sources with total mass up to 800 $\mathrm{M}_\odot$ and expands the range of targeted mass ratio q to between $1/1 - 1/10$. We also further explore the effects of the component spins on detection efficiency. Of the 43 targeted IMBH sources, 4 have spins aligned with the orbital axis, with effective total spin (Ajith et al. 2011) $\chi_{\mathrm{eff}} \equiv (\chi_{1,\parallel} + q\chi_{2,\parallel})/(1+q) = 0.8$, where $\chi_\parallel$ denotes the BH spin resolved along the orbital axis, and 4 have anti-aligned spins with $\chi_{\mathrm{eff}} = -0.8$. A further 11 have precessing spins: $\chi_{\mathrm{p}} \neq 0$, where χ_{p} is the effective spin-precession parameter of Hannam et al. (2014); Schmidt et al. (2015).

The simulated signals for each targeted source point are uniformly distributed in sky location (θ, ϕ) and inclination angle $\cos(\iota)$. The source redshift z is uniformly distributed in comoving volume, according to the TT+lowP+lensing+ext cosmological parameters given in Table IV of Ade et al. (2016), up to a maximum redshift z_{max}. The signals are added to the O3 strain data, i.e. injected, with a uniform spacing in time approximately every 100 s over the full observing time, $T_0 = 363.38$ days.

To avoid generating injections that are well outside any possible detection range, z_{max} is calculated for each IMBH source point independently. We consider values of redshift z in increments of 0.05 and calculate a conservative upper bound on the optimal three-detector network SNR, $\mathrm{SNR}_{\mathrm{net}}$, for each z. To bound the optimal SNR in a single detector, we assume the source is face-on $\cos(\iota) = 1$, located directly overhead the detector, and we estimate the detector's PSD using $\sim$ 8 hours of typical O3 data. For precessing waveforms, the ι is set at 10 Hz. We determine the maximum redshift by requiring that $\mathrm{SNR}_{\mathrm{net}}(z_{\mathrm{max}}) \sim 5$. This results a range of z_{max} across all targeted sources from 0.05 for the $(400+400)\,\mathrm{M}_\odot$ anti-aligned spin source to 2.75 for the $(100+100)\,\mathrm{M}_\odot$ aligned-spin source, as in Table 3.

When generating the injection parameters, we impose an additional threshold $\mathrm{SNR}_{\mathrm{net}} > 5$ to limit the number of simulations injected into detection pipelines that have a negligibly small probability of detection. For this purpose, the $\mathrm{SNR}_{\mathrm{net}}$ is re-estimated, taking into account the randomly selected source position and orientation. We thus assume simulated events with $\mathrm{SNR}_{\mathrm{net}} < 5$ are missed by the search pipelines; these events are, though, accounted for in the calculation of sensitive volume and merger rates.

As stated in Sect. 3, the searches process the remaining injections with the same configuration as used for results from O3 data. This is necessary to obtain unbiased rate estimates. In the case of cWB, injections were processed with the most sensitive two-detector configuration: thus, for consistency, we consider only events recovered in the corresponding offline two-detector search results.

M (M$_\odot$)	q	$\chi_{\rm eff}$	$\chi_{\rm p}$	SIM ID	$z_{\rm max}$	$\langle VT\rangle_{\rm sen}$ [Gpc^{3}yr]	$R_{90\%}$ [Gpc^{-3}yr^{-1}]
120	1/2	0.00	0.00	SXS:BBH:0169, RIT:BBH:0117:n140, GT:0446	2.00	12.42	0.19
120	1/4	0.00	0.00	SXS:BBH:0182, RIT:BBH:0119:n140, GT:0454	1.35	5.08	0.45
120	1/5	0.00	0.00	SXS:BBH:0056, RIT:BBH:0120:n140, GT:0906	1.15	3.45	0.67
120	1/7	0.00	0.00	SXS:BBH:0298 RIT:BBH:Q10:n173, GT:0568	0.90	1.85	1.24
120	1/10	0.00	0.00	SXS:BBH:0154, RIT:BBH:0068:n100	0.70	0.91	2.52
150	1/2	0.00	0.00	SXS:BBH:0169, RIT:BBH:0117:n140, GT:0446	1.85	12.84	0.30
200	1	0.00	0.00	SXS:BBH:0180, RIT:BBH:0198:n140, GT:0905	1.85	16.04	0.14
200	1/2	0.00	0.00	SXS:BBH:0169, RIT:BBH:0117:n140, GT:0446	1.60	11.67	0.20
200	1/4	0.00	0.00	SXS:BBH:0182, RIT:BBH:0119:n140, GT:0454	1.15	4.80	0.48
200	1/7	0.00	0.00	SXS:BBH:0298 RIT:BBH:Q10:n173, GT:0568	0.80	1.74	1.32
220	1/10	0.00	0.00	SXS:BBH:0154, RIT:BBH:0068:n100	0.60	0.81	2.86
250	1/4	0.00	0.00	SXS:BBH:0182, RIT:BBH:0119:n140, GT:0454	1.00	3.90	0.59
300	1/2	0.00	0.00	SXS:BBH:0169, RIT:BBH:0117:n140, GT:0446	1.15	7.55	0.31
350	1/6	0.00	0.00	SXS:BBH:0181, RIT:BBH:0121:n140, GT:0604	0.60	1.13	2.03
400	1	0.00	0.00	SXS:BBH:0180, RIT:BBH:0198:n140, GT:0905	1.00	5.65	0.41
400	1/2	0.00	0.00	SXS:BBH:0169, RIT:BBH:0117:n140, GT:0446	0.85	4.06	0.57
400	1/3	0.00	0.00	SXS:BBH:0030, RIT:BBH:0102:n140, GT:0453	0.70	2.55	0.90
400	1/4	0.00	0.00	SXS:BBH:0182, RIT:BBH:0119:n140, GT:0454	0.60	1.70	1.36
400	1/7	0.00	0.00	SXS:BBH:0298 RIT:BBH:Q10:n173, GT:0568	0.45	0.68	3.38
440	1/10	0.00	0.00	RIT:BBH:Q10:n173, GT:0568	0.30	0.31	7.51
500	2/3	0.00	0.00	RIT:BBH:0115:n140, GT:0477	0.70	2.39	0.96
600	1	0.00	0.00	SXS:BBH:0180, RIT:BBH:0198:n140, GT:0905	0.55	1.09	2.12
600	1/2	0.00	0.00	SXS:BBH:0169, RIT:BBH:0117:n140, GT:0446	0.50	0.99	2.32
800	1	0.00	0.00	SXS:BBH:0180, RIT:BBH:0198:n140, GT:0905	0.35	0.20	11.76
200	1	0.80	0.00	SXS:BBH:0230, RIT:BBH:0063:n100	2.75	40.34	0.06
400	1	0.80	0.00	SXS:BBH:0230, RIT:BBH:0063:n100	1.55	20.07	0.11
600	1	0.80	0.00	SXS:BBH:0230, RIT:BBH:0063:n100	0.95	6.46	0.36
800	1	0.80	0.00	SXS:BBH:0230, RIT:BBH:0063:n100	0.65	1.36	1.70
200	1	-0.80	0.00	SXS:BBH:0154,RIT:BBH:0068:n100	1.45	11.40	0.20
400	1	-0.80	0.00	SXS:BBH:0154,RIT:BBH:0068:n100	0.75	2.33	0.99
600	1	-0.80	0.00	SXS:BBH:0154,RIT:BBH:0068:n100	0.40	0.29	7.88
800	1	-0.80	0.00	SXS:BBH:0154,RIT:BBH:0068:n100	0.25	0.06	38.27
200	1	0.51	0.42	GT:0803	2.15	27.72	0.08
200	1/2	0.14	0.42	GT:0872	1.90	15.45	0.15
200	1/4	0.26	0.42	GT:0875	1.55	9.20	0.25
200	1/7	0.32	0.42	GT:0888	1.15	4.30	0.54
400	1	0.51	0.42	GT:0803	1.20	11.79	0.20
400	1/2	0.14	0.42	GT:0872	1.05	6.45	0.36
400	1/4	0.26	0.42	GT:0875	0.90	4.28	0.54
400	1/7	0.32	0.42	GT:0888	0.70	2.12	1.08
600	1	0.51	0.42	GT:0803	0.70	3.02	0.76
600	1/2	0.14	0.42	GT:0872	0.60	1.73	1.33
800	1	0.51	0.42	GT:0803	0.45	0.22	10.28

Table 3. Summary of the source frame parameters, sensitive volume-time and merger rate density upper limit at 90% confidence. For the upper limit, we assume no detection except for the non-spinning system with total mass $M_T = 150\,\mathrm{M}_\odot$ and $q = 1/2$ marked with †, for which we have assumed one detection. The source spin parameters are defined at a starting frequency of 16 Hz. The gravitational waveforms are selected based on their availability.

5.2. Sensitive Volume Time and Merger Rate

Here we calculate limits on the merger rate for points in the binary component mass and spin parameter space described in Table 3, using the loudest-event method (Biswas et al. 2009; Abbott et al. 2016c).

To derive the upper limit on merger rate for a given point in source parameter space, we consider the sensitive volume-time, $\langle VT\rangle_{\rm sen}$, of our combined search to such sources at a p-value threshold of 0.251, which is determined by 200214_224526, the most significant event due to noise in the combined search results. For mergers with given intrinsic parameters the expected number of detected signals N is related to the merger rate R and to the sensitive volume-time as $\langle N\rangle = R\langle VT\rangle_{\rm sen}$. For each source point, we estimate $\langle VT\rangle_{\rm sen}$, as a fraction of the total volume-time out to its maximum injection redshift $z_{\rm max}$, by counting injected signals that are detected with a combined p-value below the threshold and dividing by the total number of injections generated.

Then, taking a uniform prior on R and using the Poisson probability of zero detected signals as a likelihood, we obtain the 90% credible upper limit $R_{90\%} = 2.3/\langle VT\rangle_{\rm sen}$. The only significant IMBH binary signal in the combined search results is GW190521. However, there is only one mass-spin (marked with † in Table 3) point which is consistent with both its component mass and spin $\chi_{\rm eff}$–$\chi_{\rm p}$ 90% credible regions. Therefore, for that source point, we conservatively use the Poisson probability of having one IMBH binary detection and thus take $R_{90\%} = 3.9/\langle VT\rangle_{\rm sen}$.

Injections with component masses (60+60) M$_\odot$were performed: however, since this parameter point is within the stellar-mass BBH distribution characterized in Abbott et al. (2021c), to which several heavy BBH systems detected in O3a may contribute, we do not quote an upper rate limit. We do, however, state search sensitivity for such systems in our data release products.

Table 3 summarises the sensitive volume-time and upper limit on the merger rate for our chosen set of injections. For simulated non-spinning sources, the sensitive volume-time de-

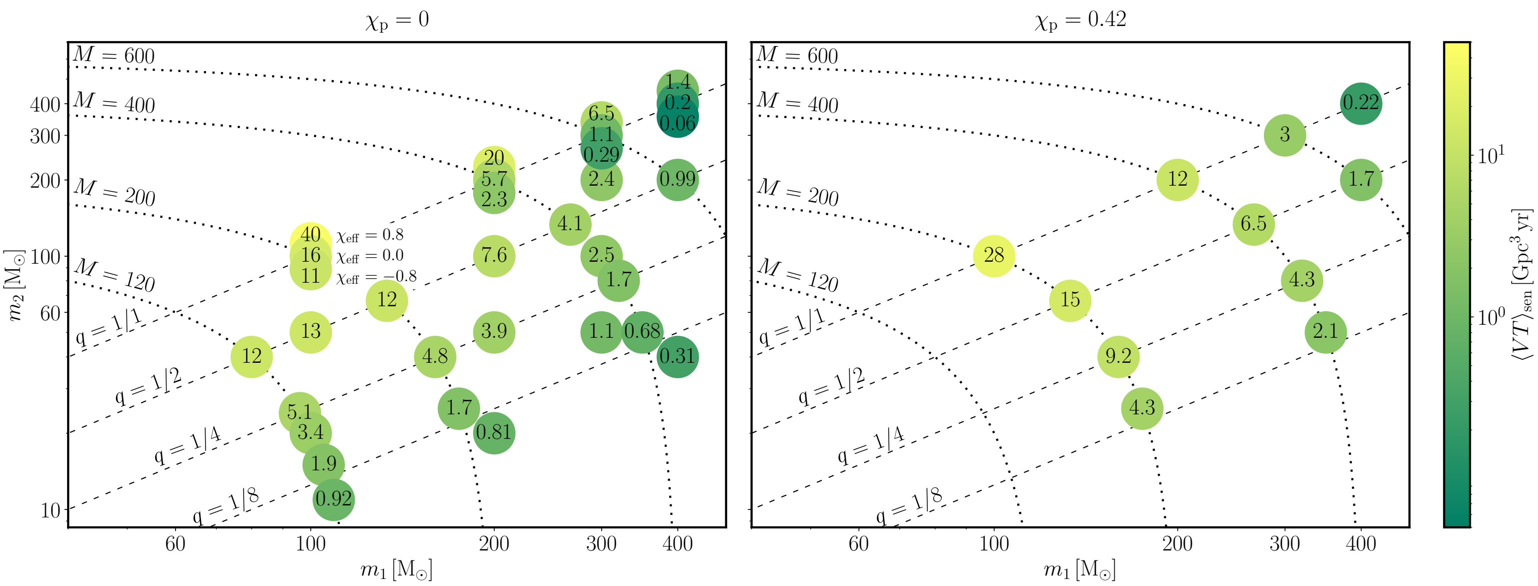

Fig. 1. The averaged sensitive time-volume $\langle VT\rangle_{sen}$ in Gpc^3 yr for the targeted IMBH binary sources in the m_1-m_2 plane. The values are rounded where necessary for display. Left panel for $\chi_p = 0$ and right panel for $\chi_p = 0.42$. Each circle corresponds to one class of IMBH binaries in the source frame. The χ_{eff} values of injection sets are labelled and shown as displaced circles.

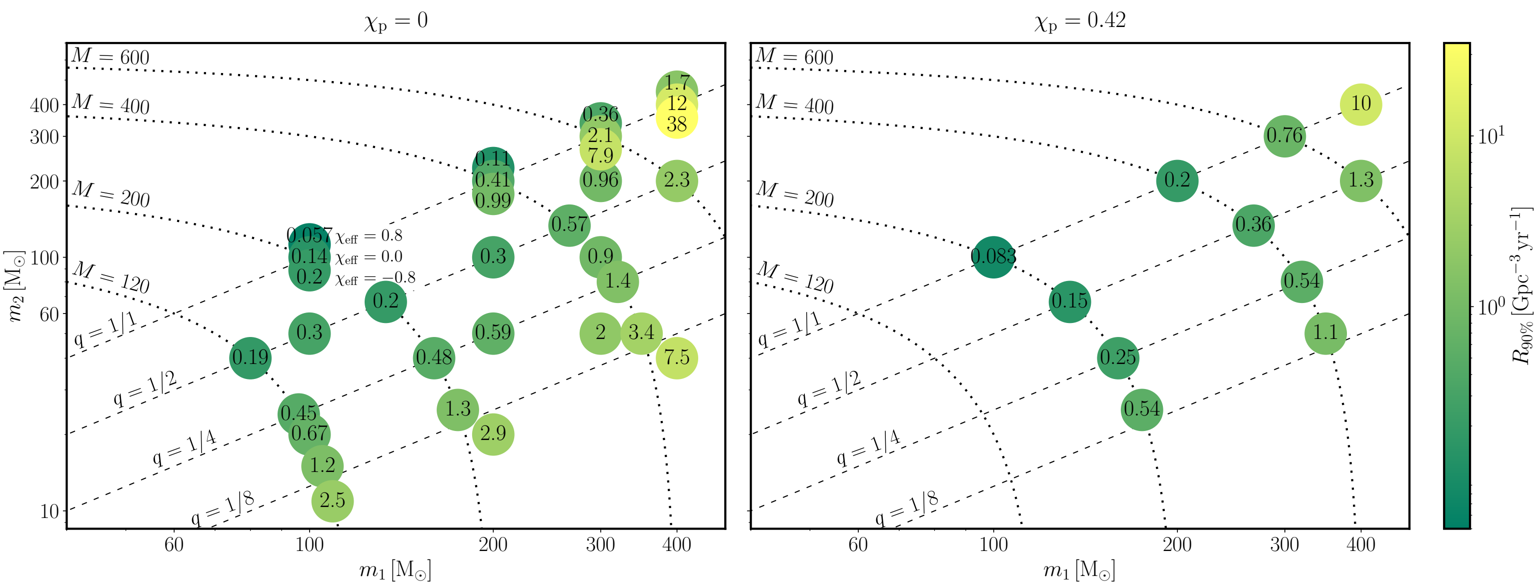

Fig. 2. The 90% upper limit on merger rate density $R_{90\%}$ in Gpc^{-3} yr^{-1} for the targeted IMBH binary sources in the m_1-m_2 plane. The values are rounded where necessary for display. Left panel for $\chi_p = 0$ and right panel for $\chi_p = 0.42$. Each circle corresponds to one class of IMBH binaries in the source frame. The χ_{eff} values of injection sets are labelled and shown as displaced circles.

creases with an increase in total mass but increases with increasing mass ratio q. There are multiple reasons for these trends. First, for a fixed mass ratio, the duration of a signal within the detector bandwidth decreases with increased total mass, even though its overall intrinsic luminosity increases. This is evident if one compares the sensitive volume-time obtained for $(80 + 40)\,M_\odot$, $(100 + 50)\,M_\odot$ and $(133 + 67)\,M_\odot$ systems. Second, the amplitude of a source decreases with a decrease in the mass ratio for a fixed total mass. Hence the sensitivity drops with a decrease in mass ratio. Last, a decrement in mass ratio also increases the contribution coming from sub-dominant emission multipoles. This significantly affects the GstLAL and PyCBC searches that filter using dominant multipole templates only.

Concerning the dependence on spins, for more positive (negative) values of the effective inspiral spin of a system, keeping the source frame component masses fixed, the duration of the merger signal within the detector bandwidth increases (decreases) as compared to a non-spinning counterpart. Also, for a binary with fixed mass and fixed non-zero effective precession spin, the total emitted GW energy is higher for aligned spins ($\chi_{eff} > 0$) as compared to anti-aligned spins ($\chi_{eff} > 0$). Hence the sensitivity improves (degrades) for systems with positive (negative) effective inspiral spin (Abbott et al. 2019; Tiwari et al. 2018). All precessing systems used in this analysis have positive χ_{eff}: hence, the combined search can observe them to a greater distance compared to their non-spinning counterpart.

Further, current searches are expected to have a higher sensitive volume for systems with aligned spins, and consequently the merger rate limits for such systems would be lower than in the case of anti-aligned spins.

Figure 1 shows this trend visually. The panels show the sensitive volume-time for non-precessing and precessing simulated sources, respectively. Each circle corresponds to one class of IMBH binaries in the source frame. The IMBH binaries with aligned and anti-aligned BH spins, $\chi_{1,2}$ are labeled and shown as displaced circles. In general, we find an increase in the sensitive volume-time of the combined search compared to results in Abbott et al. (2019). This increase is due to an overall increase in the analysis time, detector sensitivity, and the contributing searches' sensitivity.

Figure 2 shows the 90% upper limit on merger rate, $R_{90\%}$, in $\mathrm{Gpc}^{-3}\,\mathrm{yr}^{-1}$ for the targeted 43 IMBH binary sources in the m_1-m_2 plane. As before the left panel shows the result for non-precessing simulated sources whereas the right panel shows the same for precessing simulated sources. We set our most stringent upper limit 0.06 $\mathrm{Gpc}^{-3}\,\mathrm{yr}^{-1}$ for equal-mass IMBH binaries with total mass 200 $\mathrm{M}_\odot$ and spin $\chi_{1,2} = 0.8$ which is ~ 3.5 times more stringent than the previous study (Abbott et al. 2019).

5.3. Updated GW190521 merger rate estimate

We re-estimate the merger rate of a GW190521-like population. As in Abbott et al. (2017a, 2016c, 2020b,c), we consider a simulated signal to be detected if it is recovered with an FAR less than 100 yr^{-1}. This corresponds to a combined p-value threshold of 0.009. We considered the maximum observed time ($T_a = 0.874$ yr) across the three pipelines as the analysis time of the combined search. The population is generated by drawing the intrinsic parameters from the posterior distribution inferred using the `NRSur7dq4` waveform model (Abbott et al. 2020c) and then distributing them isotropically over binary orientation parameters, sky position, and uniformly over comoving volume-time up to max redshift $z = 1.5$.

The sensitive volume-time of the combined search to GW190521-like mergers over the entire O3 data is 14.35 Gpc^3 yr. As in Abbott et al. (2020c) we take a Jeffreys prior proportional to $R^{-1/2}$, where R is the astrophysical merger rate, and given the count of 1 detection above the threshold, obtain an estimate of $0.08^{+0.19}_{-0.07}\,\mathrm{Gpc}^{-3}\mathrm{yr}^{-1}$ which is more constraining than the estimate given in Abbott et al. (2020c), consistent with the higher observing time and increased sensitivity of the searches.

6. Discussion & Conclusions

The Advanced LIGO and Advanced Virgo detector network concluded their year-long third observing run in March 2020. The first part of the run witnessed a massive black hole merger event (GW190521; Abbott et al. 2020b) with a remnant firmly falling in the IMBH parameter space with the mass as $142^{+28}_{-16}\mathrm{M}_\odot$ and the components as $85^{+21}_{-14}\mathrm{M}_\odot$ and $66^{+17}_{-18}\mathrm{M}_\odot$, thus a primary BH inferred to be in the PISN mass gap. In this work, we present the IMBH binary search carried out on the entire data of the third observing run. We use three GW search algorithms for the same; the two template-based searches GstLAL and PyCBC, and one model waveform independent cWB search. The template-based matched filter searches use the dedicated template bank designed for the massive black hole binary coalescences, while the model waveform independent cWB uses a single detection approach for the entire range of BBHs masses including IMBH binaries. We rank the events based on the combined significance computed combining the three searches. The search shows that GW190521 is still the most significant IMBH binary event. Besides that, we do not find any other significant event in the combined search. We update the significance of already published O3a events with this combined search. We report the discussion on the candidate events, including the marginal events.

Amongst the remaining events, 200114_020818 shows marginal significance in the offline cWB search. As the detector characterization study does not conclusively demonstrate the origin of this event to be terrestrial, we carry out a follow-up investigation on this event in Appendix-B. This includes event reconstruction and residual analysis. While the pre-merger dynamics of 200114_020818 are barely accessible, we analyse 200114_020818 under the quasi-circular BBH hypothesis. Unlike the case of GW190521, here we find strongly inconsistent results across different waveform approximants. But the model independent event reconstructions are consistent with each other. Hence, either the event is not consistent with the available quasi-circular binary black hole waveforms or its origin is non-astrophysical in nature.

We update the merger rate density on a suite of simulated signals for IMBH binary systems with generic BH spins using the numerical relativity waveforms provided by SXS, RIT, and GeorgiaTech catalogs. With the year-long O3 data and improved sensitivity of the combined search, we compute merger rate limits using the method of loudest confirmed noise trigger. The most stringent merger rate 90% upper limit is placed on equal-mass IMBH binaries with total mass of 200 $\mathrm{M}_\odot$ and spin $\chi_{1,2} = 0.8$, as 0.056 $\mathrm{Gpc}^{-3}\mathrm{yr}^{-1}$. This is a factor ~ 3.5 below the previous limit using O1-O2 data. We further revise the astrophysical merger rate estimate for binary systems comparable to GW190521 to $0.08^{+0.19}_{-0.07}$ $\mathrm{Gpc}^{-3}\mathrm{yr}^{-1}$, a factor 1.6 more stringent than the earlier result in Abbott et al. (2020c). A semi-analytical estimate of IMBH merger rate density in globular cluster environments under certain assumptions was performed in Rasskazov et al. (2020) and Fragione et al. (2018). In this study, the calculation of expected SNR considered quadrupolar GW emission at Newtonian order from quasi-circular, non-spinning binaries; however, the inclusion of the merger and ringdown phases of the signal is expected to have a significant impact on the predicted detection rate. The observational rate upper limits obtained here can provide input to such semi-analytical approaches.

We emphasize that the IMBH binaries pose an extreme challenge to interpret. All current GW observations have been so far interpreted within the canonical scenario of an inspiraling quasi-circular BBH. While this is a safe assumption when the (pre-merger) inspiral process is clearly visible in the band, the low frequency of IMBH binary signals makes such a putative inspiral barely visible. This leaves the pre-merger dynamics and even the very nature of the colliding objects open to further interpretation, making some conclusions obtained through canonical analyses less robust (Bustillo et al. 2021a). For instance, alternative scenarios have been proposed that GW190521 is consistent with an eccentric binary merger (Romero-Shaw et al. 2020; Gayathri et al. 2020). Moreover, Bustillo et al. (2021b) have shown that GW190521 is consistent with the merger of exotic objects which has dramatically different astrophysical conclusions. The primordial BH scenario is explored by De Luca et al. (2021) and Clesse & Garcia-Bellido (2020). Alternative scenarios for forming BHs in the mass gap include gas accretion onto stellar mass BHs in dense molecular clouds, or in primordial dense clusters

(Roupas & Kazanas 2019; Safarzadeh & Haiman 2020; Rice & Zhang 2021).

With continuous improvement in the sensitivity of advanced detectors, especially in the low-frequency region, we expect to observe higher numbers of inspiral cycles from massive BBH mergers, and hence better probe inspiral dynamics, including the effects of orbital eccentricity and precession on the signal. In addition, systems with asymmetric component masses may be observed, enabling us to probe higher-order multipole emissions. Such gravitational-wave signals including higher-order multipoles and precession have a complex morphology: future developments in templated searches to incorporate such complex dynamics (Harry et al. 2018) can be expected to improve the detectability of IMBH binaries with matched-filter based methods. Similar to the current interferometer network, we expect future detector noise to include a variety of artifacts, including transients (glitches) at low frequency which may mimic some aspects of IMBH binary signals. Improved veto methods to distinguish between short-duration noise transients and IMBH signals will thus be a valuable step toward increasing the detection rate, and may benefit from novel machine learning-based classification approaches (Jadhav et al. 2020).

The detection of massive BHs in the GW window has provided crucial observations input for the stellar evolutionary models. While we use the conservative limit of the lower edge of the mass gap in the BH population, it is highly uncertain, it might be as low as $\sim 40\ M_\odot$ or above $\sim 70\ M_\odot$, depending on uncertainties about the nuclear reaction rates (e.g., Farmer et al. 2019, 2020; Costa et al. 2021), the collapse of the residual stellar envelope (e.g., Mapelli et al. 2020; Costa et al. 2021), the impact of stellar rotation (e.g., Mapelli et al. 2020; Marchant & Moriya 2020; Woosley & Heger 2021), the result of stellar mergers (e.g., Di Carlo et al. 2019, 2020b; Renzo et al. 2020a), the efficiency of accretion from companion stars (e.g., van Son et al. 2020), the model of convection (e.g., Renzo et al. 2020b; Farrell et al. 2021; Tanikawa et al. 2021) and the onset of dredge-up episodes (e.g., Costa et al. 2021; Tanikawa et al. 2021; Umeda et al. 2020). Recently, Costa et al. (2021) propose that the mass gap might even disappear if a low rate for the $^{12}C(\alpha,\gamma)^{16}O$ reaction is assumed and if a mild envelope under-shooting is included in stellar evolution calculations. Theoretical and numerical models show that black holes with mass in the pair instability gap could be the result of hierarchical mergers of smaller black holes (Miller & Hamilton 2002; Antonini & Rasio 2016; Gerosa & Berti 2017; Fishbach et al. 2017; Rodriguez et al. 2019; Kimball et al. 2021; Doctor et al. 2020) or the outcome of stellar collisions in dense star clusters (Di Carlo et al. 2019, 2020a; Kremer et al. 2020; Renzo et al. 2020a). Hierarchical mergers appear to be particularly efficient in nuclear star clusters (Antonini et al. 2019; Fragione et al. 2020; Baibhav et al. 2020; Mapelli et al. 2021) and in the dense gaseous disks of active galactic nuclei (McKernan et al. 2012; Bartos et al. 2017; McKernan et al. 2018; Yang et al. 2019; Tagawa et al. 2020, 2021). The detection of more massive BH binaries in the advanced detector era will provide constraints on all the formation channels. In addition, future observations of IMBH binaries across the GW spectrum (Sathyaprakash & Schutz 2009) could strengthen the possible evolutionary link between stellar-mass BHs and supermassive BHs in the galactic centres in coming decades (Mezcua 2017; Koliopanos 2017; King & Dehnen 2005).

Appendix A: Other marginal candidate events

Table A.1 summarises the other marginal candidates identified by our combined IMBH search in O3 data that are not reported elsewhere in a catalog of compact binary coalescence events and that satisfy the criteria described in Sect. 3.4. These triggers were reported by at least one of the contributing searches with a FAR below $0.5\,\mathrm{yr}^{-1}$, and have a $\bar{p} \leq 0.7$.

The event 191225_215715 was first reported by PyCBC Live (Dal Canton et al. 2020), a low-latency matched-filter search with a FAR of $0.4\,\mathrm{yr}^{-1}$. When the contributing searches conducted a dedicated offline analysis, the PyCBC-IMBH search identified it with a FAR of $0.47\,\mathrm{yr}^{-1}$. However, the cWB and GstLAL-IMBH searches did not identify the event. The transient did not pass cWB veto threshold as discussed in Sect. 3.1. The event is, though, identified by the most general cWB search for GW bursts of short duration with a FAR of $\sim 2\,\mathrm{yr}^{-1}$, which is still consistent with noise origin. The model-agnostic BayesWave (BW) analysis (Cornish & Littenberg 2015; Cornish et al. 2021) also identified the event with a FAR of $\sim 1\,\mathrm{yr}^{-1}$. The event morphologically resembles the Tomte class of glitches (Davis et al. 2021) which are common but of unknown origin. Followup of LIGO Livingston data also showed the existence of multiple comparable glitches within 100 s of the event time.

The remaining two events, 190924_232654 and 191223_014159, are likely caused by instrumental noise. In the case of 190924_232654, fast light scattering noise extending up to about 60 Hz is present in the LIGO Livingston data around the time of the event, and there is a high-SNR glitch in the Virgo data. The time-frequency morphology of the 191223_014159 signal in the LIGO Livingston data matches an instrumental glitch (Davis et al. 2021).

Appendix B: Followup studies of 200114_020818

The cWB offline search detects 200114_020818 with a combined FAR of $0.058\,\mathrm{yr}^{-1}$. The network SNR with LHO-LLO network is 12.3 and the three detector network SNR is 14.5. Although we cannot exclude the terrestrial origin of 200114_020818, we did perform several follow-up studies on this candidate which we summarise here. The studies include event reconstruction by BayesWave (BW) and cWB, parameter estimation (PE) with models of black hole binary merger including effects of orbital precession and higher-order multipole emission, reconstruction of PE sample waveforms and comparison with the event reconstruction with cWB, and residual analysis with BW.

Appendix B.1: Investigation of instrumental noise

As mentioned in Sect. 4, an instrumental noise transient at the Hanford observatory coincides with 200114_020818. The noise originates from a fan on a laser controller located on top of a squeezed light optics enclosure. At the time of the event, an accelerometer detected a second-long frequency dip in the 76 Hz fan motion. Such vibrational transients can weakly couple to the strain data through the squeezing system. We perform a follow-up investigation using the methods described in Nguyen et al. (2021) to acquire accurate estimates of the vibrational coupling between the table accelerometer and the strain channel. We estimate the expected noise in the strain channel at the fundamental frequency to be over an order of magnitude below background levels, so the fan is highly unlikely to account for the event candidate; however, the estimated noise at the first harmonic (152 Hz) is about a factor of two below background and could potentially impact parameter estimation.

Appendix B.2: Event reconstruction by model independent analysis

We reconstruct the signal using two model-independent analyses, namely cWB (used in the searches) and BW. The BW algorithm constructs the signal as a linear combination of sine-Gaussian wavelets and does not use any astrophysical model. The cWB reconstructs the multi-detector maximum likelihood signal by using the inverse wavelet transformation with selected pixels. In Fig. B.1, the red coloured solid and dotted blue curves correspond to the whitened reconstructed signal from cWB and BW respectively. The cWB event reconstruction is within the 90% credible region of the event reconstruction by BW (blue shaded region) for all three detectors. The BW SNR is 4, 14, and 5 in LHO, LLO and Virgo respectively, while cWB SNR is 5, 12, and 6 obtained from the reconstructed event.

Appendix B.3: PE analysis

Here, we investigate the possibility that 200114_020818 may be described by the merger of a quasi-circular BBH system. We thus carry out parameter estimation with up-to-date waveform models including effects of precession and higher-order multipole moments. Specifically, we use three quasi-circular BBH waveform models $h(t;\theta)$: i) the numerical relativity surrogate model `NRSur7dq4` (Varma et al. 2019); ii) the effective-one-body model `SEOBNRv4PHM` (Ossokine et al. 2020; Babak et al. 2017) and iii) the phenomenological model `IMRPhenomXPHM` (Pratten et al. 2021). We perform the analysis on 8 s of data centred around 200114_020818. All analyses were performed on C01 60Hz subtracted data with a lower cutoff frequency of 10 Hz and reference frequency of 11 Hz. For the `IMRPhenomXPHM` analysis, we use the nested sampling algorithm as implemented in LALInference (Veitch et al. 2015), while for `SEOBNRv4PHM` and `NRSur7dq4` analysis instead, we use the RIFT (Lange et al. 2017) analysis tool. Both algorithms are designed to compute the joint 15-dimensional posterior distribution $p(\theta|D,H)$. The evidence computed via Eq. 5 may be employed for model selection: the evidence for the signal hypothesis H, described by a specific model with given priors, is compared to the evidence for the null hypothesis N, according to which no signal is present, by computing the (log10) Bayes factor as given by

$$\log_{10} B_{\mathrm{SN}} = \log_{10} \frac{p(d|H)}{p(d|N)}\,. \tag{B.1}$$

The $\log_{10} B_{\mathrm{SN}}$ [3] is tabulated in Table B.1 for all the three runs. The values of $\log_{10} B_{\mathrm{SN}}$ indicate a preference for the hypothesis H that a signal is present over the alternative of only Gaussian noise.

These results do not, though, address the possibility that excess power in one or more detectors may be due to an instrumental artifact (glitch). As a diagnostic we therefore perform a *coherence test* (Veitch & Vecchio 2008), using the `IMRPhenomXPHM` waveform model. The coherence test computes the Bayes factor for the coherent signal hypothesis against the hypothesis of an incoherent signal in the network of detectors. It can be thus interpreted loosely as an indicator of the presence of accidentally coincident noise artefacts that could mimic

[3] The uncertainties on the individual $\log_{10} B_{\mathrm{SN}}$ are ~ 1.

Event	GPS Time (s)	cWB FAR (yr^{-1})	PyCBC FAR (yr^{-1})	GstLAL FAR (yr^{-1})	$\bar{p}$
190924_232654	1253402832.9	-	$9.0 \times 10^{+1}$	4.0×10^{-1}	6.5×10^{-1}
191225_215715	1261346253.8	-	4.7×10^{-1}	$2.0 \times 10^{+3}$	6.5×10^{-1}
191223_014159	1261100537.6	-	-	4.6×10^{-1}	7.0×10^{-1}

Table A.1. Other marginal candidate event list. We find 3 candidate events that passed a FAR threshold of $0.5\,\mathrm{yr}^{-1}$ in at least one of the three dedicated searches, and additionally have a combined p-value less than 0.7.

an astrophysical signal. The resulting $\log_{10}$ Bayes factor for coherent vs. incoherent signal 0.2, providing little to no evidence in support of the coherent signal hypothesis. Such small evidence is easily understood by looking at the $\log_{10}$ Bayes factors computed from analyses of each individual detector's data: both a Hanford-only as well as Virgo only analysis recovers a $\log_{10}$ Bayes factor for the signal vs. Gaussian noise hypothesis of 0.2. As a consequence, the posterior distributions from the Hanford- and Virgo-only analyses are largely uninformative. On the other hand, a Livingston-only analysis finds a $\log_{10}$ Bayes factor of 25. Hence, from the parameter estimation point of view, 200114_020818 is essentially a single detector event. Returning to the results under the hypothesis H of a quasi-circular merger signal plus Gaussian noise, we summarise the resulting median and symmetric 90% credible regions for a few astrophysically relevant parameters from each of the models in Table B.1.

Fig. B.2 shows the joint posterior distribution for the component masses m_1 and m_2 of the source according to each waveform model. The three models infer BH masses that are largely inconsistent. In particular, the inferred values – median and 90% credible intervals – show little overlap, see Table B.1. Moreover, the result from `SEOBNRv4PHM` shows a hint of bimodality in the mass posterior distributions.

The posterior distributions for the spin parameters, Fig. B.2, tell a similar story. If we compare the joint posterior distributions for the effective spin parameter χ_{eff} along the direction of the orbital angular momentum and the in-plane effective spin parameter χ_{p}, we find that `IMRPhenomXPHM` and `SEOBNRv4PHM` probability distributions that are disjoint at the 90% credible level. `NRSur7dq4` instead recovers a posterior distribution that is much broader and encompasses both the posterior from `IMRPhenomXPHM` and `SEOBNRv4PHM`. With reference to Table B.1, all the three results indicate a preference towards the system being precessing and with their spin vectors anti-aligned compared to the orbital angular momentum. Spin vectors anti-aligned with the orbital angular momentum have the effect of accelerating the dynamical evolution of the system towards coalescence, resulting in shorter GW signals for a given chirp mass.

In summary, a follow-up investigation of the properties of 200114_020818 interpreted as a possible quasi-circular binary merger shows considerable inconsistencies between results obtained by different waveform models. This is exemplified by the different posterior distributions for the BH masses as well as for their spins. Together with the lack of coherence among different detectors, our analysis indicates that, while we cannot exclude that 200114_020818 has an astrophysical origin, there is no consistent support for its interpretation as a quasi-circular binary merger.

Appendix B.4: Residual analysis

We evaluate the consistency of parameter estimation using the `IMRPhenomXPHM` waveform via two further analyses with BW. We obtain a match between the BW event reconstruction waveform with the maximum likelihood waveform from the `IMRPhenomXPHM` PE study as 0.871 which is consistent with expectations (Ghonge et al. 2020). Further, we perform a signal residual test by subtracting the maximum likelihood `IMRPhenomXPHM` waveform from the data and analyze the resulting residual with BW: the SNR obtained from the subtracted data is 7.4 for the LLO-LHO-Virgo network. In parallel, we estimate the distribution of SNR expected in noise from different time segments of O3 data. We estimate a p-value of 0.31 by comparing the distribution of noise SNRs with the actual event residual value. This study does not show significant evidence for excess noise.

Appendix B.5: Comparison between event reconstruction and injection recovery with PE samples

Here, we compare the cWB reconstructed waveforms of the event against the waveforms estimated by the PE analysis (Szczepańczyk et al. 2021; Gayathri et al. 2020; Salemi et al. 2019). We inject the waveforms corresponding to the PE samples into O3 data, estimate the reconstructed waveform for each of these samples using cWB and compare it with the reconstructed event by cWB. In Figure B.1, the grey shaded belts are 90% confidence intervals obtained with the cWB reconstruction of PE samples for each waveform. We observe that the cWB (solid red) and BW event (dashed blue) reconstructions are largely within this grey shaded belt. Further, we note that the time-domain reconstruction with the `SEOBNRv4PHM` and `NRSur7dq4` samples have broader error belts as compared to the reconstruction with the `IMRPhenomXPHM` samples. This is possibly due to broad posteriors and errors in cWB reconstruction.

To quantify the consistency between the cWB reconstruction and PE waveforms, we first compute the *null distribution* as the overlap between a injected waveform from the posterior distribution and its reconstructed waveform from the cWB. The source distribution is the distribution of the overlap between injected waveform from the posterior sample and the cWB event reconstruction of 200114_020818. The spread in the null distribution owes to the cWB reconstruction, noise fluctuation and the posterior distribution. The spread in source distribution shows disagreement between the cWB event reconstruction and injected waveform from the posterior distribution. If the PE samples accurately describe any event, we expect a significant intersection between these two distributions. The p-value of the null distribution is the fraction of samples in the null distribution with the overlap below the overlap value of the maximum likelihood waveform with the reconstructed event. The p-values for 200114_020818 are 0.01%, 0.4% and 48% corresponding to `SEOBNRv4PHM`, `NRSur7dq4` and `IMRPhenomXPHM` posterior samples, with source overlaps for the maximum likelihood waveforms of 0.5, 0.68 and 0.86 respectively. Thus, the low overlaps and p-values for the `SEOBNRv4PHM` and `NRSur7dq4` waveform models indicate that these models are inconsistent with the cWB reconstruction.

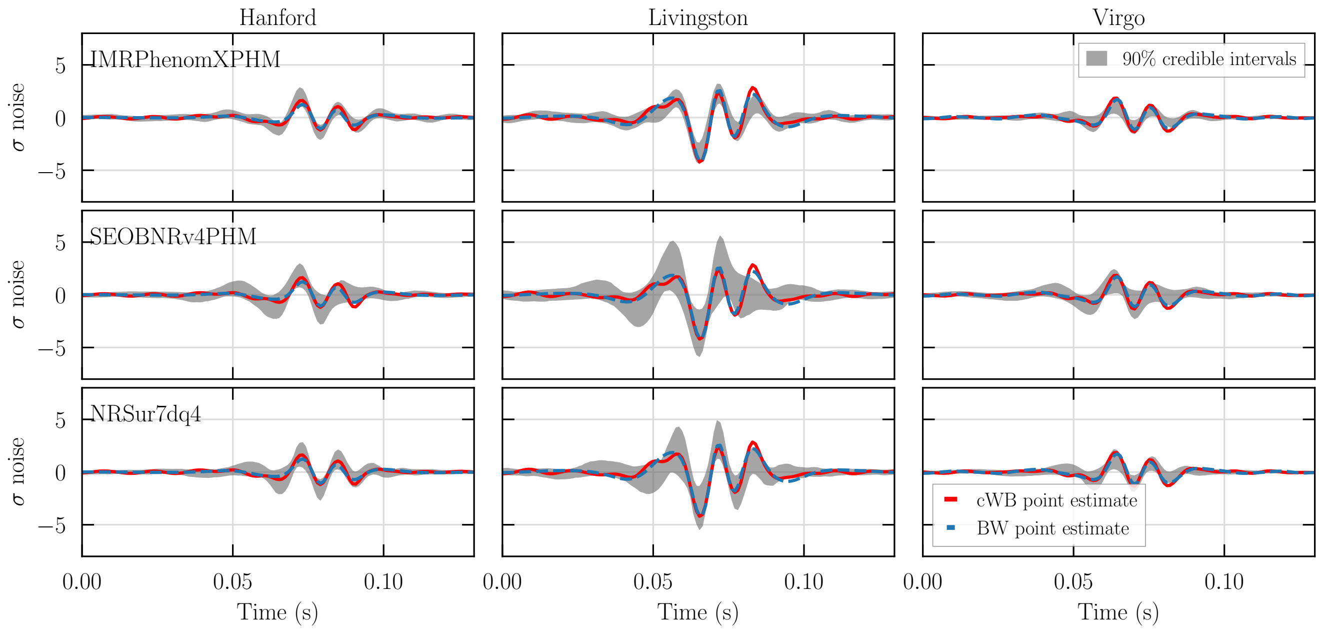

Fig. B.1. The consistency of the waveform reconstruction by cWB with three waveform models in the time domain: IMRPhenomXPHM (upper panel), SEOBNRv4PHM (middle panel), and NRSur7dq4 (lower panel). The coloured solid red and dashed blue curves correspond to the whitened reconstructed event by cWB and Bayeswave respectively. The blue shaded region corresponds to the 90% credible region from the event construction by BW. The grey shaded belts are reconstructed waveforms by cWB for the 90% credible interval corresponding to the PE runs.

Waveform Model	m_1 ($M_\odot$)	m_2 ($M_\odot$)	$\chi_{\rm eff}$	$\chi_{\rm p}$	D_L (Mpc)	$\theta_{\rm JN}$	$\log_{10} B_{SN}$
`IMRPhenomXPHM`	$197.2^{+22.6}_{-31.2}$	$62.1^{+11.1}_{-16.6}$	$-0.3^{+0.1}_{-0.2}$	$0.6^{+0.1}_{-0.2}$	$593.4^{+276.8}_{-146.7}$	$0.9^{+0.8}_{-0.3}$	24.9
`SEOBNRv4PHM`	$179.6^{+17.1}_{-60.4}$	$26.7^{+7.3}_{-6.4}$	$-0.7^{+0.2}_{-0.1}$	$0.2^{+0.3}_{-0.2}$	$475.6^{+199.1}_{-153.0}$	$1.6^{+1.2}_{-1.1}$	26.2
`NRSur7dq4`	$75.0^{+32.9}_{-18.8}$	$42.5^{+16.4}_{-18.0}$	$-0.5^{+0.3}_{-0.2}$	$0.5^{+0.3}_{-0.3}$	$1797.0^{+1601.0}_{-1027.0}$	$2.0^{+0.9}_{-1.6}$	22.3

Table B.1. Summary of median and 90% credible intervals of 200114_020818 for different waveform models. The columns show the waveform model used for parameter estimation, the source frame component masses m_i, effective spin parameters $\chi_{\rm eff}$ and $\chi_{\rm p}$, luminosity distance D_L, the angle between the total angular momentum and the direction of propagation of the gravitational wave signal $\theta_{\rm JN}$ and the $\log_{10}$ Bayes Factor between the signal and Gaussian Noise given the model.

In a separate study, we inject `IMRPhenomXPHM` PE samples and recover the simulated events with cWB using the LHO-LLO and three detector networks. We observe 25% and 34% injection recovery in LHO-LLO and LHO-LLO-Virgo configuration respectively. The three detector network is recovering more events compared to the LHO-LLO network since LHO-LLO has blind/null spots in the sky. If the LHO-LLO-Virgo network saw the same population of signals as LHO-LLO network, then we would not re-analyze the data with the LHO-LLO-Virgo network. 73% of the recovered injections by the three detector configuration is not recovered by LHO-LLO. However, out of the 34% of samples recovered by the LHO-LLO-Virgo analysis, only 8.65% of these samples have the same or higher significance than the 200114_020818 event. When we look at the detector network sensitivity skymaps, we find that it is not surprising that this event is missed by the LHO-LLO network. We conclude that the significance estimated for 200114_020818 is unlikely to result from a quasi-circular BBH with binary parameters according to `IMRPhenomXPHM`.

The detailed analyses of 200114_020818 under the quasi-circular BBH merger hypothesis gives inconsistent results across different waveform approximants with precession and higher-order multipole moments. This along with the residual study indicates that there is no consistent interpretation of the signal with the available quasi-circular merger waveforms. However, the unmodeled event reconstructions are consistent with each other. Hence, either the event is not consistent with the available quasi-circular binary black hole waveforms or its origin is non-astrophysical in nature. We do not report any alternate scenario such as eccentric binary merger due to lack of availability of waveforms which include both eccentricity and orbital precession.

Appendix C: The LIGO Scientific Collaboration, the Virgo Collaboration, and the KAGRA Collaboration

R. Abbott,[1] T. D. Abbott,[2] F. Acernese,[3,4] K. Ackley,[5] C. Adams,[6] N. Adhikari,[7] R. X. Adhikari,[1] V. B. Adya,[8] C. Affeldt,[9,10] D. Agarwal,[11] M. Agathos,[12,13] K. Agatsuma,[14] N. Aggarwal,[15] O. D. Aguiar,[16] L. Aiello,[17] A. Ain,[18] P. Ajith,[19] T. Akutsu,[20,21] S. Albanesi,[22] A. Allocca,[23,4] P. A. Altin,[8] A. Amato,[24] C. Anand,[5] S. Anand,[1] A. Ananyeva,[1] S. B. Anderson,[1] W. G. Anderson,[7] M. Ando,[25,26] T. Andrade,[27] N. Andres,[28] T. Andrić,[29] S. V. Angelova,[30] S. Ansoldi,[31,32] J. M. Antelis,[33] S. Antier,[34] S. Appert,[1] Koji Arai,[1] Koya Arai,[35] Y. Arai,[35] S. Araki,[36] A. Araya,[37] M. C. Araya,[1] J. S. Areeda,[38] M. Arène,[34] N. Aritomi,[25] N. Arnaud,[39,40] S. M. Aronson,[2] K. G. Arun,[41] H. Asada,[42] Y. Asali,[43]

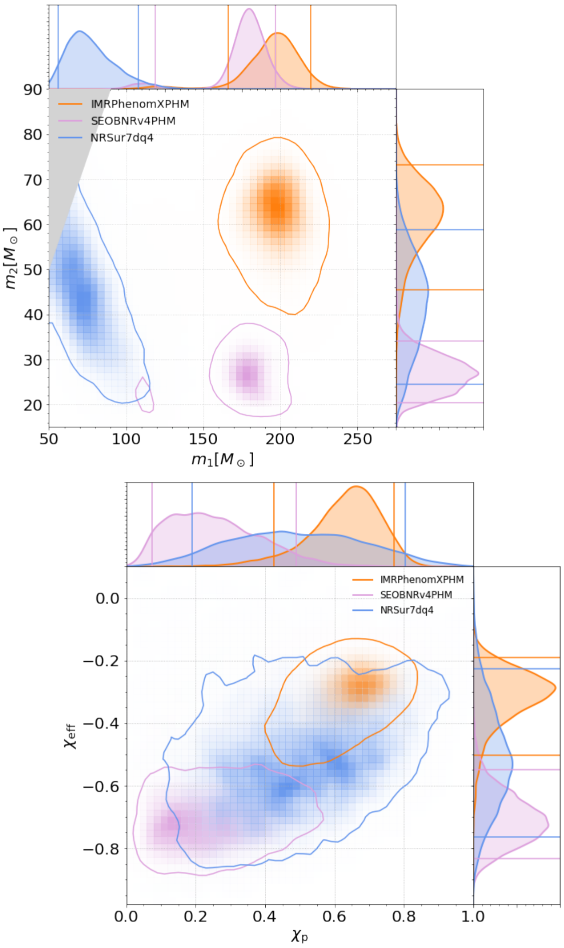

Fig. B.2. Posterior distributions: (Left) Source masses distribution, and (Right) the effective spin and effective in-plane spin distribution of 200114_020818 for different waveform models. The 90% credible regions are indicated by the solid contour in the joint distribution and by solid vertical and horizontal lines in the marginalized distributions.

G. Ashton,[5] Y. Aso,[44,45] M. Assiduo,[46,47] S. M. Aston,[6] P. Astone,[48] F. Aubin,[28] C. Austin,[2] S. Babak,[34] F. Badaracco,[49] M. K. M. Bader,[50] C. Badger,[51] S. Bae,[52] Y. Bae,[53] A. M. Baer,[54] S. Bagnasco,[22] Y. Bai,[1] L. Baiotti,[55] J. Baird,[34] R. Bajpai,[56] M. Ball,[57] G. Ballardin,[40] S. W. Ballmer,[58] A. Balsamo,[54] G. Baltus,[59] S. Banagiri,[60] D. Bankar,[11] J. C. Barayoga,[1] C. Barbieri,[61,62,63] B. C. Barish,[1] D. Barker,[64] P. Barneo,[27] F. Barone,[65,4] B. Barr,[66] L. Barsotti,[67] M. Barsuglia,[34] D. Barta,[68] J. Bartlett,[64] M. A. Barton,[66,20] I. Bartos,[69] R. Bassiri,[70] A. Basti,[71,18] M. Bawaj,[72,73] J. C. Bayley,[66] A. C. Baylor,[7] M. Bazzan,[74,75] B. Bécsy,[76] V. M. Bedakihale,[77] M. Bejger,[78] I. Belahcene,[39] V. Benedetto,[79] D. Beniwal,[80] T. F. Bennett,[81] J. D. Bentley,[14] M. BenYaala,[30] F. Bergamin,[9,10] S. Bernuzzi,[13] C. P. L. Berry,[15,66] D. Bersanetti,[82] A. Bertolini,[50] J. Betzwieser,[6] D. Beveridge,[83] R. Bhandare,[84] U. Bhardwaj,[85,50] D. Bhattacharjee,[86] S. Bhaumik,[69] I. A. Bilenko,[87] G. Billingsley,[1] S. Bini,[88,89] R. Birney,[90] O. Birnholtz,[91] S. Biscans,[1,67] M. Bischi,[46,47] S. Biscoveanu,[67] A. Bisht,[9,10] B. Biswas,[11] M. Bitossi,[40,18] M.-A. Bizouard,[92] J. K. Blackburn,[1] C. D. Blair,[83,6] D. G. Blair,[83] R. M. Blair,[64] F. Bobba,[93,94] N. Bode,[9,10] M. Boer,[92] G. Bogaert,[92] M. Boldrini,[95,48] L. D. Bonavena,[74] F. Bondu,[96] E. Bonilla,[70] R. Bonnand,[28] P. Booker,[9,10] B. A. Boom,[50] R. Bork,[1] V. Boschi,[18] N. Bose,[97] S. Bose,[11] V. Bossilkov,[83] V. Boudart,[59] Y. Bouffanais,[74,75] A. Bozzi,[40] C. Bradaschia,[18] P. R. Brady,[7] A. Bramley,[6] A. Branch,[6] M. Branchesi,[29,98] J. E. Brau,[57] M. Breschi,[13] T. Briant,[99] J. H. Briggs,[66] A. Brillet,[92] M. Brinkmann,[9,10] P. Brockill,[7] A. F. Brooks,[1] J. Brooks,[40] D. D. Brown,[80] S. Brunett,[1] G. Bruno,[49] R. Bruntz,[54] J. Bryant,[14] T. Bulik,[100] H. J. Bulten,[50] A. Buonanno,[101,102] R. Buscicchio,[14] D. Buskulic,[28] C. Buy,[103] R. L. Byer,[70] L. Cadonati,[104] G. Cagnoli,[24] C. Cahillane,[64] J. Calderón Bustillo,[105,106] J. D. Callaghan,[66] T. A. Callister,[107,108] E. Calloni,[23,4] J. Cameron,[83] J. B. Camp,[109] M. Canepa,[110,82] S. Canevarolo,[111] M. Cannavacciuolo,[93] K. C. Cannon,[112] H. Cao,[80] Z. Cao,[113] E. Capocasa,[20] E. Capote,[58] G. Carapella,[93,94] F. Carbognani,[40] J. B. Carlin,[114] M. F. Carney,[15] M. Carpinelli,[115,116,40] G. Carrillo,[57] G. Carullo,[71,18] T. L. Carver,[17] J. Casanueva Diaz,[40] C. Casentini,[117,118] G. Castaldi,[119] S. Caudill,[50,111] M. Cavaglià,[86] F. Cavalier,[39] R. Cavalieri,[40] M. Ceasar,[120] G. Cella,[18] P. Cerdá-Durán,[121] E. Cesarini,[118] W. Chaibi,[92] K. Chakravarti,[11] S. Chalathadka Subrahmanya,[122] E. Champion,[123] C.-H. Chan,[124] C. Chan,[112] C. L. Chan,[106] K. Chan,[106] M. Chan,[125] K. Chandra,[97] P. Chanial,[40] S. Chao,[124] P. Charlton,[126] E. A. Chase,[15] E. Chassande-Mottin,[34] C. Chatterjee,[83] Debarati Chatterjee,[11] Deep Chatterjee,[7] M. Chaturvedi,[84] S. Chaty,[34] C. Chen,[127,128] H. Y. Chen,[67] J. Chen,[124] K. Chen,[129] X. Chen,[83] Y.-B. Chen,[130] Y.-R. Chen,[131] Z. Chen,[17] H. Cheng,[69] C. K. Cheong,[106] H. Y. Cheung,[106] H. Y. Chia,[69] F. Chiadini,[132,94] C-Y. Chiang,[133] G. Chiarini,[75] R. Chierici,[134] A. Chincarini,[82] M. L. Chiofalo,[71,18] A. Chiummo,[40] G. Cho,[135] H. S. Cho,[136] R. K. Choudhary,[83] S. Choudhary,[11] N. Christensen,[92] H. Chu,[129] Q. Chu,[83] Y-K. Chu,[133] S. Chua,[8] K. W. Chung,[51] G. Ciani,[74,75] P. Ciecielag,[78] M. Cieślar,[78] M. Cifaldi,[117,118] A. A. Ciobanu,[80] R. Ciolfi,[137,75] F. Cipriano,[92] A. Cirone,[110,82] F. Clara,[64] E. N. Clark,[138] J. A. Clark,[1,104] L. Clarke,[139] P. Clearwater,[140] S. Clesse,[141] F. Cleva,[92] E. Coccia,[29,98] E. Codazzo,[29] P.-F. Cohadon,[99] D. E. Cohen,[39] L. Cohen,[2] M. Colleoni,[142] C. G. Collette,[143] A. Colombo,[61] M. Colpi,[61,62] C. M. Compton,[64] M. Constancio Jr.,[16] L. Conti,[75] S. J. Cooper,[14] P. Corban,[6] T. R. Corbitt,[2] I. Cordero-Carrión,[144] S. Corezzi,[73,72] K. R. Corley,[43] N. Cornish,[76] D. Corre,[39] A. Corsi,[145] S. Cortese,[40] C. A. Costa,[16] R. Cotesta,[102] M. W. Coughlin,[60] J.-P. Coulon,[92] S. T. Countryman,[43] B. Cousins,[146] P. Couvares,[1] D. M. Coward,[83] M. J. Cowart,[6] D. C. Coyne,[1] R. Coyne,[147] J. D. E. Creighton,[7] T. D. Creighton,[148] A. W. Criswell,[60] M. Croquette,[99] S. G. Crowder,[149] J. R. Cudell,[59] T. J. Cullen,[2] A. Cumming,[66] R. Cummings,[66] L. Cunningham,[66] E. Cuoco,[40,150,18] M. Curyło,[100] P. Dabadie,[24] T. Dal Canton,[39] S. Dall'Osso,[29] G. Dálya,[151] A. Dana,[70] L. M. DaneshgaranBajastani,[81] B. D'Angelo,[110,82] S. Danilishin,[152,50] S. D'Antonio,[118] K. Danzmann,[9,10] C. Darsow-Fromm,[122] A. Dasgupta,[77] L. E. H. Datrier,[66] S. Datta,[11] V. Dattilo,[40] I. Dave,[84] M. Davier,[39] G. S. Davies,[153] D. Davis,[1] M. C. Davis,[120] E. J. Daw,[154] R. Dean,[120] D. DeBra,[70] M. Deenadayalan,[11] J. Degallaix,[155] M. De Laurentis,[23,4] S. Deléglise,[99] V. Del Favero,[123] F. De Lillo,[49] N. De Lillo,[66] W. Del Pozzo,[71,18] L. M. DeMarchi,[15] F. De Matteis,[117,118] V. D'Emilio,[17] N. Demos,[67] T. Dent,[105] A. Depasse,[49] R. De Pietri,[156,157] R. De Rosa,[23,4] C. De Rossi,[40] R. DeSalvo,[119] R. De Simone,[132] S. Dhurandhar,[11] M. C. Díaz,[148] M. Diaz-Ortiz Jr.,[69] N. A. Didio,[58] T. Dietrich,[102,50] L. Di Fiore,[4] C. Di Fronzo,[14] C. Di Giorgio,[93,94] F. Di Giovanni,[121] M. Di Giovanni,[29] T. Di Girolamo,[23,4] A. Di Lieto,[71,18] B. Ding,[143] S. Di Pace,[95,48] I. Di Palma,[95,48] F. Di Renzo,[71,18] A. K. Divakarla,[69] A. Dmitriev,[14] Z. Doctor,[57] L. D'Onofrio,[23,4] F. Donovan,[67]

K. L. Dooley,[17] S. Doravari,[11] I. Dorrington,[17] M. Drago,[95,48] J. C. Driggers,[64] Y. Drori,[1] J.-G. Ducoin,[39] P. Dupej,[66] O. Durante,[93,94] D. D'Urso,[115,116] P.-A. Duverne,[39] S. E. Dwyer,[64] C. Eassa,[64] P. J. Easter,[5] M. Ebersold,[158] T. Eckhardt,[122] G. Eddolls,[66] B. Edelman,[57] T. B. Edo,[1] O. Edy,[153] A. Effler,[6] S. Eguchi,[125] J. Eichholz,[8] S. S. Eikenberry,[69] M. Eisenmann,[28] R. A. Eisenstein,[67] A. Ejlli,[17] E. Engelby,[38] Y. Enomoto,[25] L. Errico,[23,4] R. C. Essick,[159] H. Estellés,[142] D. Estevez,[160] Z. Etienne,[161] T. Etzel,[1] M. Evans,[67] T. M. Evans,[6] B. E. Ewing,[146] V. Fafone,[117,118,29] H. Fair,[58] S. Fairhurst,[17] A. M. Farah,[159] S. Farinon,[82] B. Farr,[57] W. M. Farr,[107,108] N. W. Farrow,[5] E. J. Fauchon-Jones,[17] G. Favaro,[74] M. Favata,[162] M. Fays,[59] M. Fazio,[163] J. Feicht,[1] M. M. Fejer,[70] E. Fenyvesi,[68,164] D. L. Ferguson,[165] A. Fernandez-Galiana,[67] I. Ferrante,[71,18] T. A. Ferreira,[16] F. Fidecaro,[71,18] P. Figura,[100] I. Fiori,[40] M. Fishbach,[15] R. P. Fisher,[54] R. Fittipaldi,[166,94] V. Fiumara,[167,94] R. Flaminio,[28,168] E. Floden,[60] H. Fong,[112] J. A. Font,[121,169] B. Fornal,[170] P. W. F. Forsyth,[8] A. Franke,[122] S. Frasca,[95,48] F. Frasconi,[18] C. Frederick,[171] J. P. Freed,[33] Z. Frei,[151] A. Freise,[172] R. Frey,[57] P. Fritschel,[67] V. V. Frolov,[6] G. G. Fronzé,[22] Y. Fujii,[173] Y. Fujikawa,[174] M. Fukunaga,[35] M. Fukushima,[21] P. Fulda,[69] M. Fyffe,[6] H. A. Gabbard,[66] W. Gabella,[207] B. U. Gadre,[102] J. R. Gair,[102] J. Gais,[106] S. Galaudage,[5] R. Gamba,[13] D. Ganapathy,[67] A. Ganguly,[19] D. Gao,[175] S. G. Gaonkar,[11] B. Garaventa,[82,110] C. García-Núñez,[90] C. García-Quirós,[142] F. Garufi,[23,4] B. Gateley,[64] S. Gaudio,[33] V. Gayathri,[69] G.-G. Ge,[175] G. Gemme,[82] A. Gennai,[18] J. George,[84] O. Gerberding,[122] L. Gergely,[176] P. Gewecke,[122] S. Ghonge,[104] Abhirup Ghosh,[102] Archisman Ghosh,[177] Shaon Ghosh,[7,162] Shrobana Ghosh,[17] B. Giacomazzo,[61,62,63] L. Giacoppo,[95,48] J. A. Giaime,[2,6] K. D. Giardina,[6] D. R. Gibson,[90] C. Gier,[30] M. Giesler,[178] P. Giri,[18,71] F. Gissi,[79] J. Glanzer,[2] A. E. Gleckl,[38] P. Godwin,[146] E. Goetz,[179] R. Goetz,[69] N. Gohlke,[9,10] B. Goncharov,[5,29] G. González,[2] A. Gopakumar,[180] M. Gosselin,[40] R. Gouaty,[28] D. W. Gould,[8] B. Grace,[8] A. Grado,[181,4] M. Granata,[155] V. Granata,[93] A. Grant,[66] S. Gras,[67] P. Grassia,[1] C. Gray,[64] R. Gray,[66] G. Greco,[72] A. C. Green,[69] R. Green,[17] A. M. Gretarsson,[33] E. M. Gretarsson,[33] D. Griffith,[1] W. Griffiths,[17] H. L. Griggs,[104] G. Grignani,[73,72] A. Grimaldi,[88,89] S. J. Grimm,[29,98] H. Grote,[17] S. Grunewald,[102] P. Gruning,[39] D. Guerra,[121] G. M. Guidi,[46,47] A. R. Guimaraes,[2] G. Guixé,[27] H. K. Gulati,[77] H.-K. Guo,[170] Y. Guo,[50] Anchal Gupta,[1] Anuradha Gupta,[182] P. Gupta,[50,111] E. K. Gustafson,[1] R. Gustafson,[183] F. Guzman,[184] S. Ha,[185] L. Haegel,[34] A. Hagiwara,[35,186] S. Haino,[133] O. Halim,[32,187] E. D. Hall,[67] E. Z. Hamilton,[158] G. Hammond,[66] W.-B. Han,[188] M. Haney,[158] J. Hanks,[64] C. Hanna,[146] M. D. Hannam,[17] O. Hannuksela,[111,50] H. Hansen,[64] T. J. Hansen,[33] J. Hanson,[6] T. Harder,[92] T. Hardwick,[2] K. Haris,[50,111] J. Harms,[29,98] G. M. Harry,[189] I. W. Harry,[153] D. Hartwig,[122] K. Hasegawa,[35] B. Haskell,[78] R. K. Hasskew,[6] C.-J. Haster,[67] K. Hattori,[190] K. Haughian,[66] H. Hayakawa,[191] K. Hayama,[125] F. J. Hayes,[66] J. Healy,[123] A. Heidmann,[99] A. Heidt,[9,10] M. C. Heintze,[6] J. Heinze,[9,10] J. Heinzel,[192] H. Heitmann,[92] F. Hellman,[193] P. Hello,[39] A. F. Helmling-Cornell,[57] G. Hemming,[40] M. Hendry,[66] I. S. Heng,[66] E. Hennes,[50] J. Hennig,[194] M. H. Hennig,[194] A. G. Hernandez,[81] F. Hernandez Vivanco,[5] M. Heurs,[9,10] S. Hild,[152,50] P. Hill,[30] Y. Himemoto,[195] A. S. Hines,[184] Y. Hiranuma,[196] N. Hirata,[20] E. Hirose,[35] S. Hochheim,[9,10] D. Hofman,[155] J. N. Hohmann,[122] D. G. Holcomb,[120] N. A. Holland,[8] K. Holley-Bockelmann,[207] I. J. Hollows,[154] Z. J. Holmes,[80] K. Holt,[6] D. E. Holz,[159] Z. Hong,[197] P. Hopkins,[17] J. Hough,[66] S. Hourihane,[130] E. J. Howell,[83] C. G. Hoy,[17] D. Hoyland,[14] A. Hreibi,[9,10] B-H. Hsieh,[35] Y. Hsu,[124] G-Z. Huang,[197] H-Y. Huang,[133] P. Huang,[175] Y-C. Huang,[131] Y.-J. Huang,[133] Y. Huang,[67] M. T. Hübner,[5] A. D. Huddart,[139] B. Hughey,[33] D. C. Y. Hui,[198] V. Hui,[28] S. Husa,[142] S. H. Huttner,[66] R. Huxford,[146] T. Huynh-Dinh,[6] S. Ide,[199] B. Idzkowski,[100] A. Iess,[117,118] B. Ikenoue,[21] S. Imam,[197] K. Inayoshi,[200] C. Ingram,[80] Y. Inoue,[129] K. Ioka,[201] M. Isi,[67] K. Isleif,[122] K. Ito,[202] Y. Itoh,[203,204] B. R. Iyer,[19] K. Izumi,[205] V. JaberianHamedan,[83] T. Jacqmin,[99] S. J. Jadhav,[206] S. P. Jadhav,[11] A. L. James,[17] A. Z. Jan,[123] K. Jani,[207] J. Janquart,[111,50] K. Janssens,[208,92] N. N. Janthalur,[206] P. Jaranowski,[209] D. Jariwala,[69] R. Jaume,[142] A. C. Jenkins,[51] K. Jenner,[80] C. Jeon,[210] M. Jeunon,[60] W. Jia,[67] H.-B. Jin,[211,212] G. R. Johns,[54] A. W. Jones,[83] D. I. Jones,[213] J. D. Jones,[64] P. Jones,[14] R. Jones,[66] R. J. G. Jonker,[50] L. Ju,[83] P. Jung,[53] k. Jung,[185] J. Junker,[9,10] V. Juste,[160] K. Kaihotsu,[202] T. Kajita,[214] M. Kakizaki,[215] C. V. Kalaghatgi,[17,111] V. Kalogera,[15] B. Kamai,[1] M. Kamiizumi,[191] N. Kanda,[203,204] S. Kandhasamy,[11] G. Kang,[216] J. B. Kanner,[1] Y. Kao,[124] S. J. Kapadia,[19] D. P. Kapasi,[8] S. Karat,[1] C. Karathanasis,[217] S. Karki,[86] R. Kashyap,[146] M. Kasprzack,[1] W. Kastaun,[9,10] S. Katsanevas,[40] E. Katsavounidis,[67] W. Katzman,[6] T. Kaur,[83] K. Kawabe,[64] K. Kawaguchi,[35] N. Kawai,[218] T. Kawasaki,[25] F. Kéfélian,[92] D. Keitel,[142] J. S. Key,[219] S. Khadka,[70] F. Y. Khalili,[87] S. Khan,[17] E. A. Khazanov,[220] N. Khetan,[29,98] M. Khursheed,[84] N. Kijbunchoo,[8] C. Kim,[221] J. C. Kim,[222] J. Kim,[223] K. Kim,[224] W. S. Kim,[225] Y.-M. Kim,[226] C. Kimball,[15] N. Kimura,[186] M. Kinley-Hanlon,[66] R. Kirchhoff,[9,10] J. S. Kissel,[64] N. Kita,[25] H. Kitazawa,[202] L. Kleybolte,[122] S. Klimenko,[69] A. M. Knee,[179] T. D. Knowles,[161] E. Knyazev,[67] P. Koch,[9,10] G. Koekoek,[50,152] Y. Kojima,[227] K. Kokeyama,[228] S. Koley,[29] P. Kolitsidou,[17] M. Kolstein,[217] K. Komori,[67,25] V. Kondrashov,[1] A. K. H. Kong,[229] A. Kontos,[230] N. Koper,[9,10] M. Korobko,[122] K. Kotake,[125] M. Kovalam,[83] D. B. Kozak,[1] C. Kozakai,[44] R. Kozu,[191] V. Kringel,[9,10] N. V. Krishnendu,[9,10] A. Królak,[231,232] G. Kuehn,[9,10] F. Kuei,[124] P. Kuijer,[50] A. Kumar,[206] P. Kumar,[178] Rahul Kumar,[64] Rakesh Kumar,[77] J. Kume,[26] K. Kuns,[67] C. Kuo,[129] H-S. Kuo,[197] Y. Kuromiya,[202] S. Kuroyanagi,[233,234] K. Kusayanagi,[218] S. Kuwahara,[112] K. Kwak,[185] P. Lagabbe,[28] D. Laghi,[71,18] E. Lalande,[235] T. L. Lam,[106] A. Lamberts,[92,236] M. Landry,[64] B. B. Lane,[67] R. N. Lang,[67] J. Lange,[165] B. Lantz,[70] I. La Rosa,[28] A. Lartaux-Vollard,[39] P. D. Lasky,[5] M. Laxen,[6] A. Lazzarini,[1] C. Lazzaro,[74,75] P. Leaci,[95,48] S. Leavey,[9,10] Y. K. Lecoeuche,[179] H. K. Lee,[237] H. M. Lee,[135] H. W. Lee,[222] J. Lee,[135] K. Lee,[238] R. Lee,[131] J. Lehmann,[9,10] A. Lemaître,[239] M. Leonardi,[20] N. Leroy,[39] N. Letendre,[28] C. Levesque,[235] Y. Levin,[5] J. N. Leviton,[183] K. Leyde,[34] A. K. Y. Li,[1] B. Li,[124] J. Li,[15] K. L. Li,[240] T. G. F. Li,[106] X. Li,[130] C-Y. Lin,[241] F-K. Lin,[133] F-L. Lin,[197] H. L. Lin,[129] L. C.-C. Lin,[185] F. Linde,[242,50] S. D. Linker,[81] J. N. Linley,[66] T. B. Littenberg,[243] G. C. Liu,[127] J. Liu,[9,10] K. Liu,[124] X. Liu,[7] F. Llamas,[148] M. Llorens-Monteagudo,[121] R. K. L. Lo,[1] A. Lockwood,[244] L. T. London,[67] A. Longo,[245,246] D. Lopez,[158] M. Lopez Portilla,[111] M. Lorenzini,[117,118] V. Loriette,[247] M. Lormand,[6] G. Losurdo,[18] T. P. Lott,[104] J. D. Lough,[9,10] C. O. Lousto,[123] G. Lovelace,[38] J. F. Lucaccioni,[171] H. Lück,[9,10] D. Lumaca,[117,118] A. P. Lundgren,[153] L.-W. Luo,[133] J. E. Lynam,[54] R. Macas,[153] M. MacInnis,[67] D. M. Macleod,[17] I. A. O. MacMillan,[1] A. Macquet,[92] I. Magaña Hernandez,[7] C. Magazzù,[18] R. M. Magee,[1] R. Maggiore,[14] M. Magnozzi,[82,110] S. Mahesh,[161] E. Majorana,[95,48] C. Makarem,[1] I. Maksimovic,[247] S. Maliakal,[1] A. Malik,[84] N. Man,[92] V. Mandic,[60] V. Mangano,[95,48]

J. L. Mango,[248] G. L. Mansell,[64,67] M. Manske,[7] M. Mantovani,[40] M. Mapelli,[74,75] F. Marchesoni,[249,72,250] M. Marchio,[20] F. Marion,[28] Z. Mark,[130] S. Márka,[43] Z. Márka,[43] C. Markakis,[12] A. S. Markosyan,[70] A. Markowitz,[1] E. Maros,[1] A. Marquina,[144] S. Marsat,[34] F. Martelli,[46,47] I. W. Martin,[66] R. M. Martin,[162] M. Martinez,[217] V. A. Martinez,[69] V. Martinez,[24] K. Martinovic,[51] D. V. Martynov,[14] E. J. Marx,[67] H. Masalehdan,[122] K. Mason,[67] E. Massera,[154] A. Masserot,[28] T. J. Massinger,[67] M. Masso-Reid,[66] S. Mastrogiovanni,[34] A. Matas,[102] M. Mateu-Lucena,[142] F. Matichard,[1,67] M. Matiushechkina,[9,10] N. Mavalvala,[67] J. J. McCann,[83] R. McCarthy,[64] D. E. McClelland,[8] P. K. McClincy,[146] S. McCormick,[6] L. McCuller,[67] G. I. McGhee,[66] S. C. McGuire,[251] C. McIsaac,[153] J. McIver,[179] T. McRae,[8] S. T. McWilliams,[161] D. Meacher,[7] M. Mehmet,[9,10] A. K. Mehta,[102] Q. Meijer,[111] A. Melatos,[114] D. A. Melchor,[38] G. Mendell,[64] A. Menendez-Vazquez,[217] C. S. Menoni,[163] R. A. Mercer,[7] L. Mereni,[155] K. Merfeld,[57] E. L. Merilh,[6] J. D. Merritt,[57] M. Merzougui,[92] S. Meshkov*,[1] C. Messenger,[66] C. Messick,[165] P. M. Meyers,[114] F. Meylahn,[9,10] A. Mhaske,[11] A. Miani,[88,89] H. Miao,[14] I. Michaloliakos,[69] C. Michel,[155] Y. Michimura,[25] H. Middleton,[114] L. Milano,[23] A. L. Miller,[49] A. Miller,[81] B. Miller,[85,50] M. Millhouse,[114] J. C. Mills,[17] E. Milotti,[187,32] O. Minazzoli,[92,252] Y. Minenkov,[118] N. Mio,[253] Ll. M. Mir,[217] M. Miravet-Tenés,[121] C. Mishra,[254] T. Mishra,[69] T. Mistry,[154] S. Mitra,[11] V. P. Mitrofanov,[87] G. Mitselmakher,[69] R. Mittleman,[67] O. Miyakawa,[191] A. Miyamoto,[203] Y. Miyazaki,[25] K. Miyo,[191] S. Miyoki,[191] Geoffrey Mo,[67] E. Moguel,[171] K. Mogushi,[86] S. R. P. Mohapatra,[67] S. R. Mohite,[7] I. Molina,[38] M. Molina-Ruiz,[193] M. Mondin,[81] M. Montani,[46,47] C. J. Moore,[14] D. Moraru,[64] F. Morawski,[78] A. More,[11] C. Moreno,[33] G. Moreno,[64] Y. Mori,[202] S. Morisaki,[7] Y. Moriwaki,[215] B. Mours,[160] C. M. Mow-Lowry,[14,172] S. Mozzon,[153] F. Muciaccia,[95,48] Arunava Mukherjee,[255] D. Mukherjee,[146] Soma Mukherjee,[148] Subroto Mukherjee,[77] Suvodip Mukherjee,[85] N. Mukund,[9,10] A. Mullavey,[6] J. Munch,[80] E. A. Muñiz,[58] P. G. Murray,[66] R. Musenich,[82,110] S. Muusse,[80] S. L. Nadji,[9,10] K. Nagano,[205] S. Nagano,[256] A. Nagar,[22,257] K. Nakamura,[20] H. Nakano,[258] M. Nakano,[35] R. Nakashima,[218] Y. Nakayama,[202] V. Napolano,[40] I. Nardecchia,[117,118] T. Narikawa,[35] L. Naticchioni,[48] B. Nayak,[81] R. K. Nayak,[259] R. Negishi,[196] B. F. Neil,[83] J. Neilson,[79,94] G. Nelemans,[260] T. J. N. Nelson,[6] M. Nery,[9,10] P. Neubauer,[171] A. Neunzert,[219] K. Y. Ng,[67] S. W. S. Ng,[80] C. Nguyen,[34] P. Nguyen,[57] T. Nguyen,[67] L. Nguyen Quynh,[261] W.-T. Ni,[211,175,131] S. A. Nichols,[2] A. Nishizawa,[26] S. Nissanke,[85,50] E. Nitoglia,[134] F. Nocera,[40] M. Norman,[17] C. North,[17] S. Nozaki,[190] L. K. Nuttall,[153] J. Oberling,[64] B. D. O'Brien,[69] Y. Obuchi,[21] J. O'Dell,[139] E. Oelker,[66] W. Ogaki,[35] G. Oganesyan,[29,98] J. J. Oh,[225] K. Oh,[198] S. H. Oh,[225] M. Ohashi,[191] N. Ohishi,[44] M. Ohkawa,[174] F. Ohme,[9,10] H. Ohta,[112] M. A. Okada,[16] Y. Okutani,[199] K. Okutomi,[191] C. Olivetto,[40] K. Oohara,[196] C. Ooi,[25] R. Oram,[6] B. O'Reilly,[6] R. G. Ormiston,[60] N. D. Ormsby,[54] L. F. Ortega,[69] R. O'Shaughnessy,[123] E. O'Shea,[178] S. Oshino,[191] S. Ossokine,[102] C. Osthelder,[1] S. Otabe,[218] D. J. Ottaway,[80] H. Overmier,[6] A. E. Pace,[146] G. Pagano,[71,18] M. A. Page,[83] G. Pagliaroli,[29,98] A. Pai,[97] S. A. Pai,[84] J. R. Palamos,[57] O. Palashov,[220] C. Palomba,[48] H. Pan,[124] K. Pan,[131,229] P. K. Panda,[206] H. Pang,[129] P. T. H. Pang,[50,111] C. Pankow,[15] F. Pannarale,[95,48] B. C. Pant,[84] F. H. Panther,[83] F. Paoletti,[18] A. Paoli,[40] A. Paolone,[48,262] A. Parisi,[127] H. Park,[7] J. Park,[263] W. Parker,[6,251] D. Pascucci,[50] A. Pasqualetti,[40] R. Passaquieti,[71,18] D. Passuello,[18] M. Patel,[54] M. Pathak,[80] B. Patricelli,[40,18] A. S. Patron,[2] S. Paul,[57] E. Payne,[5] M. Pedraza,[1] M. Pegoraro,[75] A. Pele,[6] F. E. Peña Arellano,[191] S. Penn,[264] A. Perego,[88,89] A. Pereira,[24] T. Pereira,[265] C. J. Perez,[64] C. Périgois,[28] C. C. Perkins,[69] A. Perreca,[88,89] S. Perriès,[134] J. Petermann,[122] D. Petterson,[1] H. P. Pfeiffer,[102] K. A. Pham,[60] K. S. Phukon,[50,242] O. J. Piccinni,[48] M. Pichot,[92] M. Piendibene,[71,18] F. Piergiovanni,[46,47] L. Pierini,[95,48] V. Pierro,[79,94] G. Pillant,[40] M. Pillas,[39] F. Pilo,[18] L. Pinard,[155] I. M. Pinto,[79,94,266] M. Pinto,[40] K. Piotrzkowski,[49] M. Pirello,[64] M. D. Pitkin,[267] E. Placidi,[95,48] L. Planas,[142] W. Plastino,[245,246] C. Pluchar,[138] R. Poggiani,[71,18] E. Polini,[28] D. Y. T. Pong,[106] S. Ponrathnam,[11] P. Popolizio,[40] E. K. Porter,[34] R. Poulton,[40] J. Powell,[140] M. Pracchia,[28] T. Pradier,[160] A. K. Prajapati,[77] K. Prasai,[70] R. Prasanna,[206] G. Pratten,[14] M. Principe,[79,266,94] G. A. Prodi,[268,89] L. Prokhorov,[14] P. Prosposito,[117,118] L. Prudenzi,[102] A. Puecher,[50,111] M. Punturo,[72] F. Puosi,[18,71] P. Puppo,[48] M. Pürrer,[102] H. Qi,[17] V. Quetschke,[148] R. Quitzow-James,[86] F. J. Raab,[64] G. Raaijmakers,[85,50] H. Radkins,[64] N. Radulesco,[92] P. Raffai,[151] S. X. Rail,[235] S. Raja,[84] C. Rajan,[84] K. E. Ramirez,[6] T. D. Ramirez,[38] A. Ramos-Buades,[102] J. Rana,[146] P. Rapagnani,[95,48] U. D. Rapol,[269] A. Ray,[7] V. Raymond,[17] N. Raza,[179] M. Razzano,[71,18] J. Read,[38] L. A. Rees,[189] T. Regimbau,[28] L. Rei,[82] S. Reid,[30] S. W. Reid,[54] D. H. Reitze,[1,69] P. Relton,[17] A. Renzini,[1] P. Rettegno,[270,22] M. Rezac,[38] F. Ricci,[95,48] D. Richards,[139] J. W. Richardson,[1] L. Richardson,[184] G. Riemenschneider,[270,22] K. Riles,[183] S. Rinaldi,[18,71] K. Rink,[179] M. Rizzo,[15] N. A. Robertson,[1,66] R. Robie,[1] F. Robinet,[39] A. Rocchi,[118] S. Rodriguez,[38] L. Rolland,[28] J. G. Rollins,[1] M. Romanelli,[96] R. Romano,[3,4] C. L. Romel,[64] A. Romero-Rodríguez,[217] I. M. Romero-Shaw,[5] J. H. Romie,[6] S. Ronchini,[29,98] L. Rosa,[4,23] C. A. Rose,[7] D. Rosińska,[100] M. P. Ross,[244] S. Rowan,[66] S. J. Rowlinson,[14] S. Roy,[111] Santosh Roy,[11] Soumen Roy,[271] D. Rozza,[115,116] P. Ruggi,[40] K. Ruiz-Rocha,[207] K. Ryan,[64] S. Sachdev,[146] T. Sadecki,[64] J. Sadiq,[105] N. Sago,[272] S. Saito,[21] Y. Saito,[191] K. Sakai,[273] Y. Sakai,[196] M. Sakellariadou,[51] Y. Sakuno,[125] O. S. Salafia,[63,62,61] L. Salconi,[40] M. Saleem,[60] F. Salemi,[88,89] A. Samajdar,[50,111] E. J. Sanchez,[1] J. H. Sanchez,[38] L. E. Sanchez,[1] N. Sanchis-Gual,[274] J. R. Sanders,[275] A. Sanuy,[27] T. R. Saravanan,[11] N. Sarin,[5] B. Sassolas,[155] H. Satari,[83] B. S. Sathyaprakash,[146,17] S. Sato,[276] T. Sato,[174] O. Sauter,[69] R. L. Savage,[64] T. Sawada,[203] D. Sawant,[97] H. L. Sawant,[11] S. Sayah,[155] D. Schaetzl,[1] M. Scheel,[130] J. Scheuer,[15] M. Schiworski,[80] P. Schmidt,[14] S. Schmidt,[111] R. Schnabel,[122] M. Schneewind,[9,10] R. M. S. Schofield,[57] A. Schönbeck,[122] B. W. Schulte,[9,10] B. F. Schutz,[17,9,10] E. Schwartz,[17] J. Scott,[66] S. M. Scott,[8] M. Seglar-Arroyo,[28] T. Sekiguchi,[26] Y. Sekiguchi,[277] D. Sellers,[6] A. S. Sengupta,[271] D. Sentenac,[40] E. G. Seo,[106] V. Sequino,[23,4] A. Sergeev,[220] Y. Setyawati,[111] T. Shaffer,[64] M. S. Shahriar,[15] B. Shams,[170] L. Shao,[200] A. Sharma,[29,98] P. Sharma,[84] P. Shawhan,[101] N. S. Shcheblanov,[239] S. Shibagaki,[125] M. Shikauchi,[112] R. Shimizu,[21] T. Shimoda,[25] K. Shimode,[191] H. Shinkai,[278] T. Shishido,[45] A. Shoda,[20] D. H. Shoemaker,[67] D. M. Shoemaker,[165] S. ShyamSundar,[84] M. Sieniawska,[100] D. Sigg,[64] L. P. Singer,[109] D. Singh,[146] N. Singh,[100] A. Singha,[152,50] A. M. Sintes,[142] V. Sipala,[115,116] V. Skliris,[17] B. J. J. Slagmolen,[8] T. J. Slaven-Blair,[83] J. Smetana,[14] J. R. Smith,[38] R. J. E. Smith,[5] J. Soldateschi,[279,280,47] S. N. Somala,[281] K. Somiya,[218] E. J. Son,[225] K. Soni,[11] S. Soni,[2] V. Sordini,[134] F. Sorrentino,[82] N. Sorrentino,[71,18] H. Sotani,[282] R. Soulard,[92] T. Souradeep,[269,11] E. Sowell,[145] V. Spagnuolo,[152,50] A. P. Spencer,[66] M. Spera,[74,75] R. Srinivasan,[92] A. K. Srivastava,[77] V. Srivastava,[58]

K. Staats,[15] C. Stachie,[92] D. A. Steer,[34] J. Steinlechner,[152,50] S. Steinlechner,[152,50] D. J. Stops,[14] M. Stover,[171] K. A. Strain,[66] L. C. Strang,[114] G. Stratta,[283,47] A. Strunk,[64] R. Sturani,[265] A. L. Stuver,[120] S. Sudhagar,[11] V. Sudhir,[67] R. Sugimoto,[284,205] H. G. Suh,[7] T. Z. Summerscales,[285] H. Sun,[83] L. Sun,[8] S. Sunil,[77] A. Sur,[78] J. Suresh,[112,35] P. J. Sutton,[17] Takamasa Suzuki,[174] Toshikazu Suzuki,[35] B. L. Swinkels,[50] M. J. Szczepańczyk,[69] P. Szewczyk,[100] M. Tacca,[50] H. Tagoshi,[35] S. C. Tait,[66] H. Takahashi,[286] R. Takahashi,[20] A. Takamori,[37] S. Takano,[25] H. Takeda,[25] M. Takeda,[203] C. J. Talbot,[30] C. Talbot,[1] H. Tanaka,[287] Kazuyuki Tanaka,[203] Kenta Tanaka,[287] Taiki Tanaka,[35] Takahiro Tanaka,[272] A. J. Tanasijczuk,[49] S. Tanioka,[20,45] D. B. Tanner,[69] D. Tao,[1] L. Tao,[69] E. N. Tapia San Martin,[20] E. N. Tapia San Martín,[50] C. Taranto,[117] J. D. Tasson,[192] S. Telada,[288] R. Tenorio,[142] J. E. Terhune,[120] L. Terkowski,[122] M. P. Thirugnanasambandam,[11] M. Thomas,[6] P. Thomas,[64] J. E. Thompson,[17] S. R. Thondapu,[84] K. A. Thorne,[6] E. Thrane,[5] Shubhanshu Tiwari,[158] Srishti Tiwari,[11] V. Tiwari,[17] A. M. Toivonen,[60] K. Toland,[66] A. E. Tolley,[153] T. Tomaru,[20] Y. Tomigami,[203] T. Tomura,[191] M. Tonelli,[71,18] A. Torres-Forné,[121] C. I. Torrie,[1] I. Tosta e Melo,[115,116] D. Töyrä,[8] A. Trapananti,[249,72] F. Travasso,[72,249] G. Traylor,[6] M. Trevor,[101] M. C. Tringali,[40] A. Tripathee,[183] L. Troiano,[289,94] A. Trovato,[34] L. Trozzo,[4,191] R. J. Trudeau,[1] D. S. Tsai,[124] D. Tsai,[124] K. W. Tsang,[50,290,111] T. Tsang,[291] J-S. Tsao,[197] M. Tse,[67] R. Tso,[130] K. Tsubono,[25] S. Tsuchida,[203] L. Tsukada,[112] D. Tsuna,[112] T. Tsutsui,[112] T. Tsuzuki,[21] K. Turbang,[292,208] M. Turconi,[92] D. Tuyenbayev,[203] A. S. Ubhi,[14] N. Uchikata,[35] T. Uchiyama,[191] R. P. Udall,[1] A. Ueda,[186] T. Uehara,[293,294] K. Ueno,[112] G. Ueshima,[295] C. S. Unnikrishnan,[180] F. Uraguchi,[21] A. L. Urban,[2] T. Ushiba,[191] A. Utina,[152,50] H. Vahlbruch,[9,10] G. Vajente,[1] A. Vajpeyi,[5] G. Valdes,[184] M. Valentini,[88,89] V. Valsan,[7] N. van Bakel,[50] M. van Beuzekom,[50] J. F. J. van den Brand,[152,296,50] C. Van Den Broeck,[111,50] D. C. Vander-Hyde,[58] L. van der Schaaf,[50] J. V. van Heijningen,[49] J. Vanosky,[1] M. H. P. M. van Putten,[297] N. van Remortel,[208] M. Vardaro,[242,50] A. F. Vargas,[114] V. Varma,[178] M. Vasúth,[68] A. Vecchio,[14] G. Vedovato,[75] J. Veitch,[66] P. J. Veitch,[80] J. Venneberg,[9,10] G. Venugopalan,[1] D. Verkindt,[28] P. Verma,[232] Y. Verma,[84] D. Veske,[43] F. Vetrano,[46] A. Viceré,[46,47] S. Vidyant,[58] A. D. Viets,[248] A. Vijaykumar,[19] V. Villa-Ortega,[105] J.-Y. Vinet,[92] A. Virtuoso,[187,32] S. Vitale,[67] T. Vo,[58] H. Vocca,[73,72] E. R. G. von Reis,[64] J. S. A. von Wrangel,[9,10] C. Vorvick,[64] S. P. Vyatchanin,[87] L. E. Wade,[171] M. Wade,[171] K. J. Wagner,[123] R. C. Walet,[50] M. Walker,[54] G. S. Wallace,[30] L. Wallace,[1] S. Walsh,[7] J. Wang,[175] J. Z. Wang,[183] W. H. Wang,[148] R. L. Ward,[8] J. Warner,[64] M. Was,[28] T. Washimi,[20] N. Y. Washington,[1] J. Watchi,[143] B. Weaver,[64] S. A. Webster,[66] M. Weinert,[9,10] A. J. Weinstein,[1] R. Weiss,[67] C. M. Weller,[244] R. Weller,[207] F. Wellmann,[9,10] L. Wen,[83] P. Weßels,[9,10] K. Wette,[8] J. T. Whelan,[123] D. D. White,[38] B. F. Whiting,[69] C. Whittle,[67] D. Wilken,[9,10] D. Williams,[66] M. J. Williams,[66] A. R. Williamson,[153] J. L. Willis,[1] B. Willke,[9,10] D. J. Wilson,[138] W. Winkler,[9,10] C. C. Wipf,[1] T. Wlodarczyk,[102] G. Woan,[66] J. Woehler,[9,10] J. K. Wofford,[123] I. C. F. Wong,[106] C. Wu,[131] D. S. Wu,[9,10] H. Wu,[131] S. Wu,[131] D. M. Wysocki,[7] L. Xiao,[1] W-R. Xu,[197] T. Yamada,[287] H. Yamamoto,[1] Kazuhiro Yamamoto,[215] Kohei Yamamoto,[287] T. Yamamoto,[191] K. Yamashita,[202] R. Yamazaki,[199] F. W. Yang,[170] L. Yang,[163] Y. Yang,[298] Yang Yang,[69] Z. Yang,[60] M. J. Yap,[8] D. W. Yeeles,[17] A. B. Yelikar,[123] M. Ying,[124] K. Yokogawa,[202] J. Yokoyama,[26,25] T. Yokozawa,[191] J. Yoo,[178] T. Yoshioka,[202] Hang Yu,[130] Haocun Yu,[67] H. Yuzurihara,[35] A. Zadrożny,[232] M. Zanolin,[33] S. Zeidler,[299] T. Zelenova,[40] J.-P. Zendri,[75] M. Zevin,[159] M. Zhan,[175] H. Zhang,[197] J. Zhang,[83] L. Zhang,[1] T. Zhang,[14] Y. Zhang,[184] C. Zhao,[83] G. Zhao,[143] Y. Zhao,[20] Yue Zhao,[170] R. Zhou,[193] Z. Zhou,[15] X. J. Zhu,[5] Z.-H. Zhu,[113] A. B. Zimmerman,[165] Y. Zlochower,[123] M. E. Zucker,[1,67] and J. Zweizig[1]

[1]LIGO Laboratory, California Institute of Technology, Pasadena, CA 91125, USA
[2]Louisiana State University, Baton Rouge, LA 70803, USA
[3]Dipartimento di Farmacia, Università di Salerno, I-84084 Fisciano, Salerno, Italy
[4]INFN, Sezione di Napoli, Complesso Universitario di Monte S. Angelo, I-80126 Napoli, Italy
[5]OzGrav, School of Physics & Astronomy, Monash University, Clayton 3800, Victoria, Australia
[6]LIGO Livingston Observatory, Livingston, LA 70754, USA
[7]University of Wisconsin-Milwaukee, Milwaukee, WI 53201, USA
[8]OzGrav, Australian National University, Canberra, Australian Capital Territory 0200, Australia
[9]Max Planck Institute for Gravitational Physics (Albert Einstein Institute), D-30167 Hannover, Germany
[10]Leibniz Universität Hannover, D-30167 Hannover, Germany
[11]Inter-University Centre for Astronomy and Astrophysics, Pune 411007, India
[12]University of Cambridge, Cambridge CB2 1TN, United Kingdom
[13]Theoretisch-Physikalisches Institut, Friedrich-Schiller-Universität Jena, D-07743 Jena, Germany
[14]University of Birmingham, Birmingham B15 2TT, United Kingdom
[15]Center for Interdisciplinary Exploration & Research in Astrophysics (CIERA), Northwestern University, Evanston, IL 60208, USA
[16]Instituto Nacional de Pesquisas Espaciais, 12227-010 São José dos Campos, São Paulo, Brazil
[17]Gravity Exploration Institute, Cardiff University, Cardiff CF24 3AA, United Kingdom
[18]INFN, Sezione di Pisa, I-56127 Pisa, Italy
[19]International Centre for Theoretical Sciences, Tata Institute of Fundamental Research, Bengaluru 560089, India
[20]Gravitational Wave Science Project, National Astronomical Observatory of Japan (NAOJ), Mitaka City, Tokyo 181-8588, Japan
[21]Advanced Technology Center, National Astronomical Observatory of Japan (NAOJ), Mitaka City, Tokyo 181-8588, Japan
[22]INFN Sezione di Torino, I-10125 Torino, Italy
[23]Università di Napoli "Federico II", Complesso Universitario di Monte S. Angelo, I-80126 Napoli, Italy
[24]Université de Lyon, Université Claude Bernard Lyon 1, CNRS, Institut Lumière Matière, F-69622 Villeurbanne, France
[25]Department of Physics, The University of Tokyo, Bunkyo-ku, Tokyo 113-0033, Japan
[26]Research Center for the Early Universe (RESCEU), The University of Tokyo, Bunkyo-ku, Tokyo 113-0033, Japan
[27]Institut de Ciències del Cosmos (ICCUB), Universitat de Barcelona, C/ Martí i Franquès 1, Barcelona, 08028, Spain
[28]Laboratoire d'Annecy de Physique des Particules (LAPP), Univ. Grenoble Alpes, Université Savoie Mont Blanc, CNRS/IN2P3, F-74941 Annecy, France
[29]Gran Sasso Science Institute (GSSI), I-67100 L'Aquila, Italy
[30]SUPA, University of Strathclyde, Glasgow G1 1XQ, United Kingdom

[31]Dipartimento di Scienze Matematiche, Informatiche e Fisiche, Università di Udine, I-33100 Udine, Italy
[32]INFN, Sezione di Trieste, I-34127 Trieste, Italy
[33]Embry-Riddle Aeronautical University, Prescott, AZ 86301, USA
[34]Université de Paris, CNRS, Astroparticule et Cosmologie, F-75006 Paris, France
[35]Institute for Cosmic Ray Research (ICRR), KAGRA Observatory, The University of Tokyo, Kashiwa City, Chiba 277-8582, Japan
[36]Accelerator Laboratory, High Energy Accelerator Research Organization (KEK), Tsukuba City, Ibaraki 305-0801, Japan
[37]Earthquake Research Institute, The University of Tokyo, Bunkyo-ku, Tokyo 113-0032, Japan
[38]California State University Fullerton, Fullerton, CA 92831, USA
[39]Université Paris-Saclay, CNRS/IN2P3, IJCLab, 91405 Orsay, France
[40]European Gravitational Observatory (EGO), I-56021 Cascina, Pisa, Italy
[41]Chennai Mathematical Institute, Chennai 603103, India
[42]Department of Mathematics and Physics, Gravitational Wave Science Project, Hirosaki University, Hirosaki City, Aomori 036-8561, Japan
[43]Columbia University, New York, NY 10027, USA
[44]Kamioka Branch, National Astronomical Observatory of Japan (NAOJ), Kamioka-cho, Hida City, Gifu 506-1205, Japan
[45]The Graduate University for Advanced Studies (SOKENDAI), Mitaka City, Tokyo 181-8588, Japan
[46]Università degli Studi di Urbino "Carlo Bo", I-61029 Urbino, Italy
[47]INFN, Sezione di Firenze, I-50019 Sesto Fiorentino, Firenze, Italy
[48]INFN, Sezione di Roma, I-00185 Roma, Italy
[49]Université catholique de Louvain, B-1348 Louvain-la-Neuve, Belgium
[50]Nikhef, Science Park 105, 1098 XG Amsterdam, Netherlands
[51]King's College London, University of London, London WC2R 2LS, United Kingdom
[52]Korea Institute of Science and Technology Information (KISTI), Yuseong-gu, Daejeon 34141, Korea
[53]National Institute for Mathematical Sciences, Yuseong-gu, Daejeon 34047, Korea
[54]Christopher Newport University, Newport News, VA 23606, USA
[55]International College, Osaka University, Toyonaka City, Osaka 560-0043, Japan
[56]School of High Energy Accelerator Science, The Graduate University for Advanced Studies (SOKENDAI), Tsukuba City, Ibaraki 305-0801, Japan
[57]University of Oregon, Eugene, OR 97403, USA
[58]Syracuse University, Syracuse, NY 13244, USA
[59]Université de Liège, B-4000 Liège, Belgium
[60]University of Minnesota, Minneapolis, MN 55455, USA
[61]Università degli Studi di Milano-Bicocca, I-20126 Milano, Italy
[62]INFN, Sezione di Milano-Bicocca, I-20126 Milano, Italy
[63]INAF, Osservatorio Astronomico di Brera sede di Merate, I-23807 Merate, Lecco, Italy
[64]LIGO Hanford Observatory, Richland, WA 99352, USA
[65]Dipartimento di Medicina, Chirurgia e Odontoiatria "Scuola Medica Salernitana", Università di Salerno, I-84081 Baronissi, Salerno, Italy
[66]SUPA, University of Glasgow, Glasgow G12 8QQ, United Kingdom
[67]LIGO Laboratory, Massachusetts Institute of Technology, Cambridge, MA 02139, USA
[68]Wigner RCP, RMKI, H-1121 Budapest, Konkoly Thege Miklós út 29-33, Hungary
[69]University of Florida, Gainesville, FL 32611, USA
[70]Stanford University, Stanford, CA 94305, USA
[71]Università di Pisa, I-56127 Pisa, Italy
[72]INFN, Sezione di Perugia, I-06123 Perugia, Italy
[73]Università di Perugia, I-06123 Perugia, Italy
[74]Università di Padova, Dipartimento di Fisica e Astronomia, I-35131 Padova, Italy
[75]INFN, Sezione di Padova, I-35131 Padova, Italy
[76]Montana State University, Bozeman, MT 59717, USA
[77]Institute for Plasma Research, Bhat, Gandhinagar 382428, India
[78]Nicolaus Copernicus Astronomical Center, Polish Academy of Sciences, 00-716, Warsaw, Poland
[79]Dipartimento di Ingegneria, Università del Sannio, I-82100 Benevento, Italy
[80]OzGrav, University of Adelaide, Adelaide, South Australia 5005, Australia
[81]California State University, Los Angeles, 5151 State University Dr, Los Angeles, CA 90032, USA
[82]INFN, Sezione di Genova, I-16146 Genova, Italy
[83]OzGrav, University of Western Australia, Crawley, Western Australia 6009, Australia
[84]RRCAT, Indore, Madhya Pradesh 452013, India
[85]GRAPPA, Anton Pannekoek Institute for Astronomy and Institute for High-Energy Physics, University of Amsterdam, Science Park 904, 1098 XH Amsterdam, Netherlands
[86]Missouri University of Science and Technology, Rolla, MO 65409, USA
[87]Faculty of Physics, Lomonosov Moscow State University, Moscow 119991, Russia
[88]Università di Trento, Dipartimento di Fisica, I-38123 Povo, Trento, Italy
[89]INFN, Trento Institute for Fundamental Physics and Applications, I-38123 Povo, Trento, Italy
[90]SUPA, University of the West of Scotland, Paisley PA1 2BE, United Kingdom
[91]Bar-Ilan University, Ramat Gan, 5290002, Israel
[92]Artemis, Université Côte d'Azur, Observatoire de la Côte d'Azur, CNRS, F-06304 Nice, France
[93]Dipartimento di Fisica "E.R. Caianiello", Università di Salerno, I-84084 Fisciano, Salerno, Italy
[94]INFN, Sezione di Napoli, Gruppo Collegato di Salerno, Complesso Universitario di Monte S. Angelo, I-80126 Napoli, Italy
[95]Università di Roma "La Sapienza", I-00185 Roma, Italy
[96]Univ Rennes, CNRS, Institut FOTON - UMR6082, F-3500 Rennes, France
[97]Indian Institute of Technology Bombay, Powai, Mumbai 400 076, India
[98]INFN, Laboratori Nazionali del Gran Sasso, I-67100 Assergi, Italy
[99]Laboratoire Kastler Brossel, Sorbonne Université, CNRS, ENS-Université PSL, Collège de France, F-75005 Paris, France
[100]Astronomical Observatory Warsaw University, 00-478 Warsaw, Poland
[101]University of Maryland, College Park, MD 20742, USA
[102]Max Planck Institute for Gravitational Physics (Albert Einstein Institute), D-14476 Potsdam, Germany

[103]L2IT, Laboratoire des 2 Infinis - Toulouse, Université de Toulouse, CNRS/IN2P3, UPS, F-31062 Toulouse Cedex 9, France
[104]School of Physics, Georgia Institute of Technology, Atlanta, GA 30332, USA
[105]IGFAE, Campus Sur, Universidade de Santiago de Compostela, 15782 Spain
[106]The Chinese University of Hong Kong, Shatin, NT, Hong Kong
[107]Stony Brook University, Stony Brook, NY 11794, USA
[108]Center for Computational Astrophysics, Flatiron Institute, New York, NY 10010, USA
[109]NASA Goddard Space Flight Center, Greenbelt, MD 20771, USA
[110]Dipartimento di Fisica, Università degli Studi di Genova, I-16146 Genova, Italy
[111]Institute for Gravitational and Subatomic Physics (GRASP), Utrecht University, Princetonplein 1, 3584 CC Utrecht, Netherlands
[112]RESCEU, University of Tokyo, Tokyo, 113-0033, Japan.
[113]Department of Astronomy, Beijing Normal University, Beijing 100875, China
[114]OzGrav, University of Melbourne, Parkville, Victoria 3010, Australia
[115]Università degli Studi di Sassari, I-07100 Sassari, Italy
[116]INFN, Laboratori Nazionali del Sud, I-95125 Catania, Italy
[117]Università di Roma Tor Vergata, I-00133 Roma, Italy
[118]INFN, Sezione di Roma Tor Vergata, I-00133 Roma, Italy
[119]University of Sannio at Benevento, I-82100 Benevento, Italy and INFN, Sezione di Napoli, I-80100 Napoli, Italy
[120]Villanova University, 800 Lancaster Ave, Villanova, PA 19085, USA
[121]Departamento de Astronomía y Astrofísica, Universitat de València, E-46100 Burjassot, València, Spain
[122]Universität Hamburg, D-22761 Hamburg, Germany
[123]Rochester Institute of Technology, Rochester, NY 14623, USA
[124]National Tsing Hua University, Hsinchu City, 30013 Taiwan, Republic of China
[125]Department of Applied Physics, Fukuoka University, Jonan, Fukuoka City, Fukuoka 814-0180, Japan
[126]OzGrav, Charles Sturt University, Wagga Wagga, New South Wales 2678, Australia
[127]Department of Physics, Tamkang University, Danshui Dist., New Taipei City 25137, Taiwan
[128]Department of Physics and Institute of Astronomy, National Tsing Hua University, Hsinchu 30013, Taiwan
[129]Department of Physics, Center for High Energy and High Field Physics, National Central University, Zhongli District, Taoyuan City 32001, Taiwan
[130]CaRT, California Institute of Technology, Pasadena, CA 91125, USA
[131]Department of Physics, National Tsing Hua University, Hsinchu 30013, Taiwan
[132]Dipartimento di Ingegneria Industriale (DIIN), Università di Salerno, I-84084 Fisciano, Salerno, Italy
[133]Institute of Physics, Academia Sinica, Nankang, Taipei 11529, Taiwan
[134]Université Lyon, Université Claude Bernard Lyon 1, CNRS, IP2I Lyon / IN2P3, UMR 5822, F-69622 Villeurbanne, France
[135]Seoul National University, Seoul 08826, South Korea
[136]Pusan National University, Busan 46241, South Korea
[137]INAF, Osservatorio Astronomico di Padova, I-35122 Padova, Italy
[138]University of Arizona, Tucson, AZ 85721, USA
[139]Rutherford Appleton Laboratory, Didcot OX11 0DE, United Kingdom
[140]OzGrav, Swinburne University of Technology, Hawthorn VIC 3122, Australia
[141]Université libre de Bruxelles, Avenue Franklin Roosevelt 50 - 1050 Bruxelles, Belgium
[142]Universitat de les Illes Balears, IAC3—IEEC, E-07122 Palma de Mallorca, Spain
[143]Université Libre de Bruxelles, Brussels 1050, Belgium
[144]Departamento de Matemáticas, Universitat de València, E-46100 Burjassot, València, Spain
[145]Texas Tech University, Lubbock, TX 79409, USA
[146]The Pennsylvania State University, University Park, PA 16802, USA
[147]University of Rhode Island, Kingston, RI 02881, USA
[148]The University of Texas Rio Grande Valley, Brownsville, TX 78520, USA
[149]Bellevue College, Bellevue, WA 98007, USA
[150]Scuola Normale Superiore, Piazza dei Cavalieri, 7 - 56126 Pisa, Italy
[151]MTA-ELTE Astrophysics Research Group, Institute of Physics, Eötvös University, Budapest 1117, Hungary
[152]Maastricht University, P.O. Box 616, 6200 MD Maastricht, Netherlands
[153]University of Portsmouth, Portsmouth, PO1 3FX, United Kingdom
[154]The University of Sheffield, Sheffield S10 2TN, United Kingdom
[155]Université Lyon, Université Claude Bernard Lyon 1, CNRS, Laboratoire des Matériaux Avancés (LMA), IP2I Lyon / IN2P3, UMR 5822, F-69622 Villeurbanne, France
[156]Dipartimento di Scienze Matematiche, Fisiche e Informatiche, Università di Parma, I-43124 Parma, Italy
[157]INFN, Sezione di Milano Bicocca, Gruppo Collegato di Parma, I-43124 Parma, Italy
[158]Physik-Institut, University of Zurich, Winterthurerstrasse 190, 8057 Zurich, Switzerland
[159]University of Chicago, Chicago, IL 60637, USA
[160]Université de Strasbourg, CNRS, IPHC UMR 7178, F-67000 Strasbourg, France
[161]West Virginia University, Morgantown, WV 26506, USA
[162]Montclair State University, Montclair, NJ 07043, USA
[163]Colorado State University, Fort Collins, CO 80523, USA
[164]Institute for Nuclear Research, Hungarian Academy of Sciences, Bem t'er 18/c, H-4026 Debrecen, Hungary
[165]Department of Physics, University of Texas, Austin, TX 78712, USA
[166]CNR-SPIN, c/o Università di Salerno, I-84084 Fisciano, Salerno, Italy
[167]Scuola di Ingegneria, Università della Basilicata, I-85100 Potenza, Italy
[168]Gravitational Wave Science Project, National Astronomical Observatory of Japan (NAOJ), Mitaka City, Tokyo 181-8588, Japan
[169]Observatori Astronòmic, Universitat de València, E-46980 Paterna, València, Spain
[170]The University of Utah, Salt Lake City, UT 84112, USA
[171]Kenyon College, Gambier, OH 43022, USA
[172]Vrije Universiteit Amsterdam, 1081 HV, Amsterdam, Netherlands
[173]Department of Astronomy, The University of Tokyo, Mitaka City, Tokyo 181-8588, Japan

[174]Faculty of Engineering, Niigata University, Nishi-ku, Niigata City, Niigata 950-2181, Japan
[175]State Key Laboratory of Magnetic Resonance and Atomic and Molecular Physics, Innovation Academy for Precision Measurement Science and Technology (APM), Chinese Academy of Sciences, Xiao Hong Shan, Wuhan 430071, China
[176]University of Szeged, Dóm tér 9, Szeged 6720, Hungary
[177]Universiteit Gent, B-9000 Gent, Belgium
[178]Cornell University, Ithaca, NY 14850, USA
[179]University of British Columbia, Vancouver, BC V6T 1Z4, Canada
[180]Tata Institute of Fundamental Research, Mumbai 400005, India
[181]INAF, Osservatorio Astronomico di Capodimonte, I-80131 Napoli, Italy
[182]The University of Mississippi, University, MS 38677, USA
[183]University of Michigan, Ann Arbor, MI 48109, USA
[184]Texas A&M University, College Station, TX 77843, USA
[185]Department of Physics, Ulsan National Institute of Science and Technology (UNIST), Ulju-gun, Ulsan 44919, Korea
[186]Applied Research Laboratory, High Energy Accelerator Research Organization (KEK), Tsukuba City, Ibaraki 305-0801, Japan
[187]Dipartimento di Fisica, Università di Trieste, I-34127 Trieste, Italy
[188]Shanghai Astronomical Observatory, Chinese Academy of Sciences, Shanghai 200030, China
[189]American University, Washington, D.C. 20016, USA
[190]Faculty of Science, University of Toyama, Toyama City, Toyama 930-8555, Japan
[191]Institute for Cosmic Ray Research (ICRR), KAGRA Observatory, The University of Tokyo, Kamioka-cho, Hida City, Gifu 506-1205, Japan
[192]Carleton College, Northfield, MN 55057, USA
[193]University of California, Berkeley, CA 94720, USA
[194]Maastricht University, 6200 MD, Maastricht, Netherlands
[195]College of Industrial Technology, Nihon University, Narashino City, Chiba 275-8575, Japan
[196]Graduate School of Science and Technology, Niigata University, Nishi-ku, Niigata City, Niigata 950-2181, Japan
[197]Department of Physics, National Taiwan Normal University, sec. 4, Taipei 116, Taiwan
[198]Astronomy & Space Science, Chungnam National University, Yuseong-gu, Daejeon 34134, Korea, Korea
[199]Department of Physics and Mathematics, Aoyama Gakuin University, Sagamihara City, Kanagawa 252-5258, Japan
[200]Kavli Institute for Astronomy and Astrophysics, Peking University, Haidian District, Beijing 100871, China
[201]Yukawa Institute for Theoretical Physics (YITP), Kyoto University, Sakyou-ku, Kyoto City, Kyoto 606-8502, Japan
[202]Graduate School of Science and Engineering, University of Toyama, Toyama City, Toyama 930-8555, Japan
[203]Department of Physics, Graduate School of Science, Osaka City University, Sumiyoshi-ku, Osaka City, Osaka 558-8585, Japan
[204]Nambu Yoichiro Institute of Theoretical and Experimental Physics (NITEP), Osaka City University, Sumiyoshi-ku, Osaka City, Osaka 558-8585, Japan
[205]Institute of Space and Astronautical Science (JAXA), Chuo-ku, Sagamihara City, Kanagawa 252-0222, Japan
[206]Directorate of Construction, Services & Estate Management, Mumbai 400094, India
[207]Vanderbilt University, Nashville, TN 37235, USA
[208]Universiteit Antwerpen, Prinsstraat 13, 2000 Antwerpen, Belgium
[209]University of Białystok, 15-424 Białystok, Poland
[210]Department of Physics, Ewha Womans University, Seodaemun-gu, Seoul 03760, Korea
[211]National Astronomical Observatories, Chinese Academic of Sciences, Chaoyang District, Beijing, China
[212]School of Astronomy and Space Science, University of Chinese Academy of Sciences, Chaoyang District, Beijing, China
[213]University of Southampton, Southampton SO17 1BJ, United Kingdom
[214]Institute for Cosmic Ray Research (ICRR), The University of Tokyo, Kashiwa City, Chiba 277-8582, Japan
[215]Faculty of Science, University of Toyama, Toyama City, Toyama 930-8555, Japan
[216]Chung-Ang University, Seoul 06974, South Korea
[217]Institut de Física d'Altes Energies (IFAE), Barcelona Institute of Science and Technology, and ICREA, E-08193 Barcelona, Spain
[218]Graduate School of Science, Tokyo Institute of Technology, Meguro-ku, Tokyo 152-8551, Japan
[219]University of Washington Bothell, Bothell, WA 98011, USA
[220]Institute of Applied Physics, Nizhny Novgorod, 603950, Russia
[221]Ewha Womans University, Seoul 03760, South Korea
[222]Inje University Gimhae, South Gyeongsang 50834, South Korea
[223]Department of Physics, Myongji University, Yongin 17058, Korea
[224]Korea Astronomy and Space Science Institute, Daejeon 34055, South Korea
[225]National Institute for Mathematical Sciences, Daejeon 34047, South Korea
[226]Ulsan National Institute of Science and Technology, Ulsan 44919, South Korea
[227]Department of Physical Science, Hiroshima University, Higashihiroshima City, Hiroshima 903-0213, Japan
[228]School of Physics and Astronomy, Cardiff University, Cardiff, CF24 3AA, UK
[229]Institute of Astronomy, National Tsing Hua University, Hsinchu 30013, Taiwan
[230]Bard College, 30 Campus Rd, Annandale-On-Hudson, NY 12504, USA
[231]Institute of Mathematics, Polish Academy of Sciences, 00656 Warsaw, Poland
[232]National Center for Nuclear Research, 05-400 Świerk-Otwock, Poland
[233]Instituto de Fisica Teorica, 28049 Madrid, Spain
[234]Department of Physics, Nagoya University, Chikusa-ku, Nagoya, Aichi 464-8602, Japan
[235]Université de Montréal/Polytechnique, Montreal, Quebec H3T 1J4, Canada
[236]Laboratoire Lagrange, Université Côte d'Azur, Observatoire Côte d'Azur, CNRS, F-06304 Nice, France
[237]Department of Physics, Hanyang University, Seoul 04763, Korea
[238]Sungkyunkwan University, Seoul 03063, South Korea
[239]NAVIER, École des Ponts, Univ Gustave Eiffel, CNRS, Marne-la-Vallée, France
[240]Department of Physics, National Cheng Kung University, Tainan City 701, Taiwan

[241]National Center for High-performance computing, National Applied Research Laboratories, Hsinchu Science Park, Hsinchu City 30076, Taiwan
[242]Institute for High-Energy Physics, University of Amsterdam, Science Park 904, 1098 XH Amsterdam, Netherlands
[243]NASA Marshall Space Flight Center, Huntsville, AL 35811, USA
[244]University of Washington, Seattle, WA 98195, USA
[245]Dipartimento di Matematica e Fisica, Università degli Studi Roma Tre, I-00146 Roma, Italy
[246]INFN, Sezione di Roma Tre, I-00146 Roma, Italy
[247]ESPCI, CNRS, F-75005 Paris, France
[248]Concordia University Wisconsin, Mequon, WI 53097, USA
[249]Università di Camerino, Dipartimento di Fisica, I-62032 Camerino, Italy
[250]School of Physics Science and Engineering, Tongji University, Shanghai 200092, China
[251]Southern University and A&M College, Baton Rouge, LA 70813, USA
[252]Centre Scientifique de Monaco, 8 quai Antoine Ier, MC-98000, Monaco
[253]Institute for Photon Science and Technology, The University of Tokyo, Bunkyo-ku, Tokyo 113-8656, Japan
[254]Indian Institute of Technology Madras, Chennai 600036, India
[255]Saha Institute of Nuclear Physics, Bidhannagar, West Bengal 700064, India
[256]The Applied Electromagnetic Research Institute, National Institute of Information and Communications Technology (NICT), Koganei City, Tokyo 184-8795, Japan
[257]Institut des Hautes Etudes Scientifiques, F-91440 Bures-sur-Yvette, France
[258]Faculty of Law, Ryukoku University, Fushimi-ku, Kyoto City, Kyoto 612-8577, Japan
[259]Indian Institute of Science Education and Research, Kolkata, Mohanpur, West Bengal 741252, India
[260]Department of Astrophysics/IMAPP, Radboud University Nijmegen, P.O. Box 9010, 6500 GL Nijmegen, Netherlands
[261]Department of Physics, University of Notre Dame, Notre Dame, IN 46556, USA
[262]Consiglio Nazionale delle Ricerche - Istituto dei Sistemi Complessi, Piazzale Aldo Moro 5, I-00185 Roma, Italy
[263]Korea Astronomy and Space Science Institute (KASI), Yuseong-gu, Daejeon 34055, Korea
[264]Hobart and William Smith Colleges, Geneva, NY 14456, USA
[265]International Institute of Physics, Universidade Federal do Rio Grande do Norte, Natal RN 59078-970, Brazil
[266]Museo Storico della Fisica e Centro Studi e Ricerche "Enrico Fermi", I-00184 Roma, Italy
[267]Lancaster University, Lancaster LA1 4YW, United Kingdom
[268]Università di Trento, Dipartimento di Matematica, I-38123 Povo, Trento, Italy
[269]Indian Institute of Science Education and Research, Pune, Maharashtra 411008, India
[270]Dipartimento di Fisica, Università degli Studi di Torino, I-10125 Torino, Italy
[271]Indian Institute of Technology, Palaj, Gandhinagar, Gujarat 382355, India
[272]Department of Physics, Kyoto University, Sakyou-ku, Kyoto City, Kyoto 606-8502, Japan
[273]Department of Electronic Control Engineering, National Institute of Technology, Nagaoka College, Nagaoka City, Niigata 940-8532, Japan
[274]Departamento de Matemática da Universidade de Aveiro and Centre for Research and Development in Mathematics and Applications, Campus de Santiago, 3810-183 Aveiro, Portugal
[275]Marquette University, 11420 W. Clybourn St., Milwaukee, WI 53233, USA
[276]Graduate School of Science and Engineering, Hosei University, Koganei City, Tokyo 184-8584, Japan
[277]Faculty of Science, Toho University, Funabashi City, Chiba 274-8510, Japan
[278]Faculty of Information Science and Technology, Osaka Institute of Technology, Hirakata City, Osaka 573-0196, Japan
[279]Università di Firenze, Sesto Fiorentino I-50019, Italy
[280]INAF, Osservatorio Astrofisico di Arcetri, Largo E. Fermi 5, I-50125 Firenze, Italy
[281]Indian Institute of Technology Hyderabad, Sangareddy, Khandi, Telangana 502285, India
[282]iTHEMS (Interdisciplinary Theoretical and Mathematical Sciences Program), The Institute of Physical and Chemical Research (RIKEN), Wako, Saitama 351-0198, Japan
[283]INAF, Osservatorio di Astrofisica e Scienza dello Spazio, I-40129 Bologna, Italy
[284]Department of Space and Astronautical Science, The Graduate University for Advanced Studies (SOKENDAI), Sagamihara City, Kanagawa 252-5210, Japan
[285]Andrews University, Berrien Springs, MI 49104, USA
[286]Research Center for Space Science, Advanced Research Laboratories, Tokyo City University, Setagaya, Tokyo 158-0082, Japan
[287]Institute for Cosmic Ray Research (ICRR), Research Center for Cosmic Neutrinos (RCCN), The University of Tokyo, Kashiwa City, Chiba 277-8582, Japan
[288]National Metrology Institute of Japan, National Institute of Advanced Industrial Science and Technology, Tsukuba City, Ibaraki 305-8568, Japan
[289]Dipartimento di Scienze Aziendali - Management and Innovation Systems (DISA-MIS), Università di Salerno, I-84084 Fisciano, Salerno, Italy
[290]Van Swinderen Institute for Particle Physics and Gravity, University of Groningen, Nijenborgh 4, 9747 AG Groningen, Netherlands
[291]Faculty of Science, Department of Physics, The Chinese University of Hong Kong, Shatin, N.T., Hong Kong
[292]Vrije Universiteit Brussel, Boulevard de la Plaine 2, 1050 Ixelles, Belgium
[293]Department of Communications Engineering, National Defense Academy of Japan, Yokosuka City, Kanagawa 239-8686, Japan
[294]Department of Physics, University of Florida, Gainesville, FL 32611, USA
[295]Department of Information and Management Systems Engineering, Nagaoka University of Technology, Nagaoka City, Niigata 940-2188, Japan
[296]Vrije Universiteit Amsterdam, 1081 HV Amsterdam, Netherlands
[297]Department of Physics and Astronomy, Sejong University, Gwangjin-gu, Seoul 143-747, Korea
[298]Department of Electrophysics, National Chiao Tung University, Hsinchu, Taiwan
[299]Department of Physics, Rikkyo University, Toshima-ku, Tokyo 171-8501, Japan

Acknowledgements. This material is based upon work supported by NSF's LIGO Laboratory which is a major facility fully funded by the National Science Foundation. The authors also gratefully acknowledge the support of the Science and Technology Facilities Council (STFC) of the United Kingdom, the Max-Planck-

Society (MPS), and the State of Niedersachsen/Germany for support of the construction of Advanced LIGO and construction and operation of the GEO600 detector. Additional support for Advanced LIGO was provided by the Australian Research Council. The authors gratefully acknowledge the Italian Istituto Nazionale di Fisica Nucleare (INFN), the French Centre National de la Recherche Scientifique (CNRS) and the Netherlands Organization for Scientific Research, for the construction and operation of the Virgo detector and the creation and support of the EGO consortium. The authors also gratefully acknowledge research support from these agencies as well as by the Council of Scientific and Industrial Research of India, the Department of Science and Technology, India, the Science & Engineering Research Board (SERB), India, the Ministry of Human Resource Development, India, the Spanish Agencia Estatal de Investigación, the Vicepresidència i Conselleria d'Innovació, Recerca i Turisme and the Conselleria d'Educació i Universitat del Govern de les Illes Balears, the Conselleria d'Innovació, Universitats, Ciència i Societat Digital de la Generalitat Valenciana and the CERCA Programme Generalitat de Catalunya, Spain, the National Science Centre of Poland and the Foundation for Polish Science (FNP), the Swiss National Science Foundation (SNSF), the Russian Foundation for Basic Research, the Russian Science Foundation, the European Commission, the European Regional Development Funds (ERDF), the Royal Society, the Scottish Funding Council, the Scottish Universities Physics Alliance, the Hungarian Scientific Research Fund (OTKA), the French Lyon Institute of Origins (LIO), the Belgian Fonds de la Recherche Scientifique (FRS-FNRS), Actions de Recherche Concertées (ARC) and Fonds Wetenschappelijk Onderzoek – Vlaanderen (FWO), Belgium, the Paris Île-de-France Region, the National Research, Development and Innovation Office Hungary (NKFIH), the National Research Foundation of Korea, the Natural Science and Engineering Research Council Canada, Canadian Foundation for Innovation (CFI), the Brazilian Ministry of Science, Technology, and Innovations, the International Center for Theoretical Physics South American Institute for Fundamental Research (ICTP-SAIFR), the Research Grants Council of Hong Kong, the National Natural Science Foundation of China (NSFC), the Leverhulme Trust, the Research Corporation, the Ministry of Science and Technology (MOST), Taiwan, the United States Department of Energy, and the Kavli Foundation. The authors gratefully acknowledge the support of the NSF, STFC, INFN and CNRS for provision of computational resources. This work was supported by MEXT, JSPS Leading-edge Research Infrastructure Program, JSPS Grant-in-Aid for Specially Promoted Research 26000005, JSPS Grant-in-Aid for Scientific Research on Innovative Areas 2905: JP17H06358, JP17H06361 and JP17H06364, JSPS Core-to-Core Program A. Advanced Research Networks, JSPS Grant-in-Aid for Scientific Research (S) 17H06133, the joint research program of the Institute for Cosmic Ray Research, University of Tokyo, National Research Foundation (NRF) and Computing Infrastructure Project of KISTI-GSDC in Korea, Academia Sinica (AS), AS Grid Center (ASGC) and the Ministry of Science and Technology (MoST) in Taiwan under grants including AS-CDA-105-M06, Advanced Technology Center (ATC) of NAOJ, and Mechanical Engineering Center of KEK. *We would like to thank all of the essential workers who put their health at risk during the COVID-19 pandemic, without whom we would not have been able to complete this work.*

References

Aasi, J. et al. 2014, Phys. Rev., D89, 102006
Aasi, J. et al. 2015, Class. Quantum Grav., 32, 074001
Abadie, J., Abbott, B. P., Abbott, R., et al. 2012a, Physical Review D, 85
Abadie, J. et al. 2012b, Phys. Rev., D85, 102004
Abbott, B. P. et al. 2016a, Class. Quantum Grav., 33, 134001
Abbott, B. P. et al. 2016b, Phys. Rev. Lett., 116, 221101, [Erratum: Phys. Rev. Lett. **121**, 129902 (2018)]
Abbott, B. P. et al. 2016c, Astrophys. J., 832, L21
Abbott, B. P. et al. 2017a, Phys. Rev. Lett., 119, 161101
Abbott, B. P. et al. 2017b, Phys. Rev. D, 96, 022001
Abbott, B. P. et al. 2019, Phys. Rev. D, 100, 064064
Abbott, B. P. et al. 2020a, Class. Quantum Grav., 37, 055002
Abbott, R. et al. 2020b, Phys. Rev. Lett., 125, 101102
Abbott, R. et al. 2020c, Astrophys. J. Lett., 900, L13
Abbott, R. et al. 2021a, Phys. Rev. X, 11, 021053
Abbott, R. et al. 2021b
Abbott, R. et al. 2021c, Astrophys. J. Lett., 913, L7
Abbott, R. and others. 2019, GCN, 25871, 25829, 25753, 25503, 25497, 25324, 25187, 25164, 25115, 25012, 24998, 24950, 24922, 24717, 24632, 24621, 24598, 24570, 24522, 24503, 24377, 24237, 24168, 24141, 24098, 24069
Acernese, F. et al. 2015, Class. Quantum Grav., 32, 024001
Acernese, F. et al. 2018, Class. Quant. Grav., 35, 205004
Ade, P. et al. 2016, Astron. Astrophys., 594, A13
Ajith, P. et al. 2011, Phys. Rev. Lett., 106, 241101
Allen, B. 2005, Phys. Rev. D, 71, 062001
Amaro-Seoane, P., Audley, H., Babak, S., et al. 2017, arXiv e-prints, arXiv:1702.00786
Anderson, J. & van der Marel, R. P. 2010, The Astrophysical Journal, 710, 1032–1062
Antonini, F., Gieles, M., & Gualandris, A. 2019, MNRAS, 486, 5008
Antonini, F. & Rasio, F. A. 2016, ApJ, 831, 187
Atakan Gurkan, M., Freitag, M., & Rasio, F. A. 2004, Astrophys. J., 604, 632
Babak, S., Taracchini, A., & Buonanno, A. 2017, Phys. Rev. D, 95, 024010
Bachetti, M., Harrison, F. A., Walton, D. J., et al. 2014, Nature, 514, 202
Baibhav, V., Gerosa, D., Berti, E., et al. 2020, Phys. Rev. D, 102, 043002
Barkat, Z., Rakavy, G., & Sack, N. 1967, Phys. Rev. Lett., 18, 379
Bartos, I., Kocsis, B., Haiman, Z., & M'arka, S. 2017, ApJ, 835, 165
Baumgardt, H., Hut, P., Makino, J., McMillan, S., & Portegies Zwart, S. F. 2003, Astrophys. J., 582, L21
Belczynski, K., Hirschi, R., Kaiser, E. A., et al. 2020, ApJ, 890, 113
Biswas, R., Brady, P. R., Creighton, J. D. E., & Fairhurst, S. 2009, Class. Quant. Grav., 26, 175009, [Erratum: Class.Quant.Grav. 30, 079502 (2013)]
Bohé, A. et al. 2017, Phys. Rev. D, 95, 044028
Bond, J. R., Arnett, W. D., & Carr, B. J. 1984, Astrophys. J., 280, 825
Buikema, A. et al. 2020, Phys. Rev. D, 102, 062003
Bustillo, J. C., Sanchis-Gual, N., Torres-Forné, A., & Font, J. A. 2021a, Phys. Rev. Lett., 126, 201101
Bustillo, J. C., Sanchis-Gual, N., Torres-Forné, A., et al. 2021b, Phys. Rev. Lett., 126, 081101
Cabero, M. et al. 2019, Class. Quantum Grav., 36, 155010
Calderón Bustillo, J., Clark, J. A., Laguna, P., & Shoemaker, D. 2018, Phys. Rev. Lett., 121, 191102
Calderon Bustillo, J., Evans, C., Clark, J. A., et al. 2020, Communications Physics, 3
Calderón Bustillo, J., Husa, S., Sintes, A. M., & Pürrer, M. 2016, Phys. Rev. D, 93, 084019
Campanelli, M., Lousto, C. O., Zlochower, Y., & Merritt, D. 2007, Phys. Rev. Lett., 98, 231102
Cannon, K., Caudill, S., Chan, C., et al. 2021, SoftwareX, 14, 100680
Carullo, G. et al. 2018, Phys. Rev., D98, 104020
Chandra, K., Gayathri, V., Bustillo, J. C., & Pai, A. 2020, Phys. Rev. D, 102, 044035
Chandra, K., Villa-Ortega, V., Dent, T., et al. 2021, Phys. Rev. D, 104, 042004
Clesse, S. & Garcia-Bellido, J. 2020 [arXiv:2007.06481]
Cornish, N. & Littenberg, T. 2015, Class. Quant. Grav., 32, 135012
Cornish, N. J., Littenberg, T. B., Bécsy, B., et al. 2021, Phys. Rev. D, 103, 044006
Costa, G., Bressan, A., Mapelli, M., et al. 2021, MNRAS, 501, 4514
Cseh, D., Webb, N. A., Godet, O., et al. 2015, MNRAS, 446, 3268
Dal Canton, T., Nitz, A. H., Gadre, B., et al. 2020 [arXiv:2008.07494]
Dal Canton, T. et al. 2014, Phys. Rev. D, 90, 082004
Davies, G. S., Dent, T., Tápai, M., et al. 2020, Phys. Rev. D, 102, 022004
Davis, D., Massinger, T. J., Lundgren, A. P., et al. 2019, Class. Quantum Grav., 36, 055011
Davis, D. et al. 2021, Class. Quant. Grav., 38, 135014
De Luca, V., Desjacques, V., Franciolini, G., Pani, P., & Riotto, A. 2021, Physical Review Letters, 126
Di Carlo, U. N., Giacobbo, N., Mapelli, M., et al. 2019, MNRAS, 487, 2947
Di Carlo, U. N., Mapelli, M., Bouffanais, Y., et al. 2020a, Mon. Not. Roy. Astron. Soc., 497, 1043
Di Carlo, U. N., Mapelli, M., Giacobbo, N., et al. 2020b, MNRAS, 498, 495
Doctor, Z., Wysocki, D., O'Shaughnessy, R., Holz, D. E., & Farr, B. 2020, ApJ, 893, 35
Drago, M. et al. 2020 [arXiv:2006.12604]
Driggers, J. C. et al. 2019, Phys. Rev. D, 99, 042001
Ebisuzaki, T., Makino, J., Tsuru, T. G., et al. 2001, Astrophys. J., 562, L19
Essick, R., Godwin, P., Hanna, C., Blackburn, L., & Katsavounidis, E. 2020 [arXiv:2005.12761]
Estevez, D., Lagabbe, P., Masserot, A., et al. 2020, The Advanced Virgo Photon Calibrators
Ezquiaga, J. M. & Holz, D. E. 2021, ApJ, 909, L23
Farmer, R., Renzo, M., de Mink, S. E., Fishbach, M., & Justham, S. 2020, Astrophy. Lett., 902, L36
Farmer, R., Renzo, M., de Mink, S. E., Marchant, P., & Justham, S. 2019, ApJ, 887, 53
Farrell, E., Groh, J. H., Hirschi, R., et al. 2021, MNRAS, 502, L40
Farrell, S., Webb, N., Barret, D., Godet, O., & Rodrigues, J. 2009, Nature, 460, 73
Ferrarese, L. & Ford, H. 2005, Space Science Reviews, 116, 523–624
Fishbach, M. & Holz, D. E. 2020, The Astrophysical Journal, 904, L26
Fishbach, M., Holz, D. E., & Farr, B. 2017, Astrophys. J., 840, L24
Fisher, R. P. et al. 2020 [arXiv:2008.11316]
Fowler, W. A. & Hoyle, F. 1964, Astrophys J. Suppl., 9, 201
Fragione, G., Ginsburg, I., & Kocsis, B. 2018, ApJ, 856, 92
Fragione, G., Loeb, A., & Rasio, F. A. 2020, Astrophys. J., 902, L26
Fregeau, J. M., Larson, S. L., Miller, M. C., O'Shaughnessy, R., & Rasio, F. A. 2006, The Astrophysical Journal, 646, L135
Fryer, C. L., Woosley, S. E., & Heger, A. 2001, ApJ, 550, 372
Gair, J. R., Vallisneri, M., Larson, S. L., & Baker, J. G. 2013, Living Rev. Rel., 16, 7
Gayathri, V., Bacon, P., Pai, A., et al. 2019, Phys. Rev. D, 100, 124022
Gayathri, V., Healy, J., Lange, J., et al. 2020 [arXiv:2009.05461]
Gebhardt, K., Rich, R. M., & Ho, L. C. 2005, The Astrophysical Journal, 634, 1093–1102
Gerosa, D. & Berti, E. 2017, Phys. Rev. D, 95, 124046
Ghonge, S., Chatziioannou, K., Clark, J. A., et al. 2020, Phys. Rev. D, 102, 064056
Giacobbo, N., Mapelli, M., & Spera, M. 2018, MNRAS, 474, 2959
Giersz, M., Leigh, N., Hypki, A., Lützgendorf, N., & Askar, A. 2015, MNRAS, 454, 3150
Godet, O., Barret, D., Webb, N. A., Farrell, S. A., & Gehrels, N. 2009, ApJ, 705, L109
Godwin, P., Essick, R., Hanna, C., et al. 2020 [arXiv:2010.15282]
Gonzalez, J. A., Sperhake, U., Bruegmann, B., Hannam, M., & Husa, S. 2007, Phys. Rev. Lett., 98, 091101
Graham, A. W. 2012, Astrophys. J., 746, 113
Graham, A. W. & Scott, N. 2013, Astrophys. J., 764, 151
Greene, J. E., Strader, J., & Ho, L. C. 2020, Ann. Rev. Astron. Astrophys., 58, 257
Hanna, C., Caudill, S., Messick, C., et al. 2020, Phys. Rev. D, 101, 022003
Hannam, M. et al. 2014, Phys. Rev. Lett., 113, 151101
Harry, I., Bustillo, J. C., & Nitz, A. 2018, Phys. Rev. D, 97, 023004
Healy, J., Lousto, C. O., Zlochower, Y., & Campanelli, M. 2017, Classical and Quantum Gravity, 34, 224001
Heger, A., Fryer, C. L., Woosley, S. E., Langer, N., & Hartmann, D. H. 2003, ApJ, 591, 288
Heger, A. & Woosley, S. E. 2002, ApJ, 567, 532
Inayoshi, K., Visbal, E., & Haiman, Z. 2020, ARA&A, 58, 27
Israel, G. L., Belfiore, A., Stella, L., et al. 2017, Science, 355, 817
Jadhav, S., Mukund, N., Gadre, B., Mitra, S., & Abraham, S. 2020, Improving significance of binary black hole mergers in Advanced LIGO data using deep learning : Confirmation of GW151216
Jani, K., Healy, J., Clark, J. A., et al. 2016, Classical and Quantum Gravity, 33, 204001
Jani, K., Shoemaker, D., & Cutler, C. 2020, Nature Astronomy, 4, 260
Kaaret, P., Feng, H., & Roberts, T. P. 2017, Ann. Rev. Astron. Astrophys., 55, 303
Kaaret, P., Prestwich, A. H., Zezas, A., et al. 2001, MNRAS, 321, L29
Kamaretsos, I., Hannam, M., Husa, S., & Sathyaprakash, B. S. 2012, Phys. Rev., D85, 024018
Kimball, C. et al. 2021, Astrophys. J. Lett., 915, L35
King, A. R. & Dehnen, W. 2005, Mon. Not. Roy. Astron. Soc., 357, 275
Klimenko, S. & Mitselmakher, G. 2004, Class. Quantum Grav., 21, S1819
Klimenko, S., Mohanty, S., Rakhmanov, M., & Mitselmakher, G. 2005, Phys. Rev. D, 72, 122002
Klimenko, S., Mohanty, S., Rakhmanov, M., & Mitselmakher, G. 2006, J. Phys. Conf. Ser., 32, 12
Klimenko, S., Vedovato, G., Drago, M., et al. 2011, Phys. Rev. D, 83, 102001

Klimenko, S. et al. 2016, Phys. Rev. D, 93, 042004
Koliopanos, F. 2017, 51
Kormendy, J. & Ho, L. C. 2013, Ann. Rev. Astron. Astrophys., 51, 511
Kremer, K., Spera, M., Becker, D., et al. 2020, ApJ, 903, 45
Kızıltan, B., Baumgardt, H., & Loeb, A. 2017, Nature, 542, 203–205
Lange, J. et al. 2017, Phys. Rev. D, 96, 104041
Lanzoni, B., Mucciarelli, A., Origlia, L., et al. 2013, The Astrophysical Journal, 769, 107
Lin, D., Strader, J., Carrasco, E. R., et al. 2018, Nature Astronomy, 2, 656–661
Littenberg, T. B., Kanner, J. B., Cornish, N. J., & Millhouse, M. 2016, Phys. Rev. D, 94, 044050
Lützgendorf, N., Kissler-Patig, M., Noyola, E., et al. 2011, Astronomy & Astrophysics, 533, A36
Madau, P. & Rees, M. J. 2001, ApJ, 551, L27
Mapelli, M. 2016, MNRAS, 459, 3432
Mapelli, M., Dall'Amico, M., Bouffanais, Y., et al. 2021, arXiv e-prints, arXiv:2103.05016
Mapelli, M., Spera, M., Montanari, E., et al. 2020, ApJ, 888, 76
Marchant, P. & Moriya, T. J. 2020, A&A, 640, L18
McKernan, B., Ford, K. E. S., Bellovary, J., et al. 2018, ApJ, 866, 66
McKernan, B., Ford, K. E. S., Lyra, W., & Perets, H. B. 2012, Mon. Not. Roy. Astron. Soc., 425, 460
Meidam, J., Agathos, M., Van Den Broeck, C., Veitch, J., & Sathyaprakash, B. S. 2014, Phys. Rev., D90, 064009
Messick, C., Blackburn, K., Brady, P., et al. 2017, Phys. Rev. D, 95, 042001
Mezcua, M. 2017, International Journal of Modern Physics D, 26, 1730021
Miller, M. C. 2009, Classical and Quantum Gravity, 26, 094031
Miller, M. C. & Colbert, E. J. M. 2004, International Journal of Modern Physics D, 13, 1
Miller, M. C. & Hamilton, D. P. 2002, Mon. Not. Roy. Astron. Soc., 330, 232
Mozzon, S., Nuttall, L. K., Lundgren, A., et al. 2020, Class. Quant. Grav., 37, 215014
Mroué, A. H., Scheel, M. A., Szilágyi, B., et al. 2013, Physical Review Letters, 111
Necula, V., Klimenko, S., & Mitselmakher, G. 2012, J. Phys. Conf. Ser., 363, 012032
Nguyen, P. et al. 2021, Class. Quant. Grav., 38, 145001
Nitz, A. H. 2018, Classical and Quantum Gravity, 35, 035016
Nitz, A. H. & Capano, C. D. 2021, Astrophys. J. Lett., 907, L9
Nitz, A. H., Dent, T., Dal Canton, T., Fairhurst, S., & Brown, D. A. 2017, Astrophys. J., 849, 118
Nitz, A. H., Dent, T., Davies, G. S., et al. 2019, Astrophys. J., 891, 123
Noyola, E., Gebhardt, K., & Bergmann, M. 2008, The Astrophysical Journal, 676, 1008–1015
O'Leary, R. M., Rasio, F. A., Fregeau, J. M., Ivanova, N., & O'Shaughnessy, R. 2006, ApJ, 637, 937
Ossokine, S. et al. 2020, Phys. Rev. D, 102, 044055
Owen, B. J. 1996, Phys. Rev. D, 53, 6749
Pankow, C. et al. 2018, Phys. Rev. D, 98, 084016
Pasham, D. R., Strohmayer, T. E., & Mushotzky, R. F. 2015, Nature, 513, 74
Paynter, J., Webster, R., & Thrane, E. 2021, Nature Astronomy
Pratten, G. et al. 2021, Phys. Rev. D, 103, 104056
Pürrer, M. 2016, Phys. Rev. D, 93, 064041
Rasskazov, A., Fragione, G., & Kocsis, B. 2020, ApJ, 899, 149
Remillard, R. A. & McClintock, J. E. 2006, Annual Review of Astronomy and Astrophysics, 44, 49
Renzo, M., Cantiello, M., Metzger, B. D., & Jiang, Y. F. 2020a, ApJ, 904, L13
Renzo, M., Farmer, R. J., Justham, S., et al. 2020b, MNRAS, 493, 4333
Rice, J. R. & Zhang, B. 2021, The Astrophysical Journal, 908, 59
Rodriguez, C. L., Zevin, M., Amaro-Seoane, P., et al. 2019, Phys. Rev. D, 100, 043027
Romero-Shaw, I., Lasky, P. D., Thrane, E., & Calder'on Bustillo, J. 2020, Astrophys. J., 903, L5
Roupas, Z. & Kazanas, D. 2019, Astronomy & Astrophysics, 632, L8
Sachdev, S. et al. 2019 [arXiv:1901.08580]
Safarzadeh, M. & Haiman, Z. 2020, Astrophys. J., 903, L21
Salemi, F., Milotti, E., Prodi, G. A., et al. 2019, Phys. Rev. D, 100, 042003
Sathyaprakash, B. S. & Dhurandhar, S. V. 1991, Phys. Rev. D, 44, 3819
Sathyaprakash, B. S. & Schutz, B. F. 2009, Living Reviews in Relativity, 12
Schmidt, P., Ohme, F., & Hannam, M. 2015, Phys. Rev. D, 91, 024043
Servillat, M., Farrell, S. A., Lin, D., et al. 2011, ApJ, 743, 6
Soni, S. et al. 2021 [arXiv:2103.12104]
Soria, R., Hakala, P. J., Hau, G. K. T., Gladstone, J. C., & Kong, A. K. H. 2012, MNRAS, 420, 3599
Spera, M. & Mapelli, M. 2017, MNRAS, 470, 4739
Stevenson, S., Sampson, M., Powell, J., et al. 2019, ApJ, 882, 121
Sun, L. et al. 2020, Class. Quant. Grav., 37, 225008
Szczepańczyk, M. et al. 2021, Phys. Rev. D, 103, 082002
Tagawa, H., Haiman, Z., Bartos, I., & Kocsis, B. 2020, ApJ, 899, 26
Tagawa, H., Kocsis, B., Haiman, Z., et al. 2021, ApJ, 908, 194
Tanikawa, A., Kinugawa, T., Yoshida, T., Hijikawa, K., & Umeda, H. 2021, Mon. Not. Roy. Astron. Soc., 505, 2170
Thrane, E., Lasky, P. D., & Levin, Y. 2017, Phys. Rev., D96, 102004
Tiwari, V., Fairhurst, S., & Hannam, M. 2018, Astrophys. J., 868, 140
Umeda, H., Yoshida, T., Nagele, C., & Takahashi, K. 2020, The Astrophysical Journal, 905, L21
Usman, S. A. et al. 2016, Class. Quantum Grav., 33, 215004
Vajente, G., Huang, Y., Isi, M., et al. 2020, Phys. Rev. D, 101, 042003
van den Bosch, R., de Zeeuw, T., Gebhardt, K., Noyola, E., & van de Ven, G. 2006, Astrophys. J., 641, 852
van der Marel, R. P. 2004, Coevolution of Black Holes and Galaxies, 37
van Son, L. A. C., De Mink, S. E., Broekgaarden, F. S., et al. 2020, ApJ, 897, 100
Varma, V., Field, S. E., Scheel, M. A., et al. 2019, Phys. Rev. Research., 1, 033015
Veitch, J., Raymond, V., Farr, B., et al. 2015, Phys. Rev. D, 91, 042003
Veitch, J. & Vecchio, A. 2008, Phys. Rev. D, 78, 022001
Viets, A. et al. 2018, Class. Quant. Grav., 35, 095015
Vink, J. S., Higgins, E. R., Sander, A. A. C., & Sabhahit, G. N. 2021, Mon. Not. Roy. Astron. Soc., 504, 146
Vitral, E. & Mamon, G. A. 2021, Astronomy & Astrophysics, 646, A63
Volonteri, M. 2010, Astro. and Astrphy. Rev., 18, 279
Webb, N., Cseh, D., Lenc, E., et al. 2012, Science, 337, 554
Woosley, S. E. 2017, ApJ, 836, 244
Woosley, S. E. 2019, ApJ, 878, 49
Woosley, S. E., Blinnikov, S., & Heger, A. 2007, Nature, 450, 390
Woosley, S. E. & Heger, A. 2021, Astrophys. J. Lett., 912, L31
Wysocki, D., O'Shaughnessy, R., Lange, J., & Fang, Y.-L. L. 2019, Phys. Rev. D, 99, 084026
Yang, Y., Bartos, I., Gayathri, V., et al. 2019, Phys. Rev. Lett., 123, 181101
Yunes, N. & Siemens, X. 2013, Living Rev. Rel., 16, 9
Yunes, N., Yagi, K., & Pretorius, F. 2016, Phys. Rev., D94, 084002